Single-electron counting for quantum metrology

Jukka Pekola
Low Temperature Laboratory
Aalto University, Helsinki, Finland

Ville Maisi (AALTO, MIKES), Olli-Pentti Saira (AALTO), Mikko Möttönen (AALTO), Antti Kemppinen (MIKES)
Dmitri Averin (SUNY), Yuri Pashkin (NEC), Jaw-Shen Tsai (NEC)

Sergey Lotkhov (PTB), Alexander Zorin (PTB)
Martin Gustafsson (CTH), Per Delsing (CTH)

Quantum metrology of single-electron current
NIS turnstile
Photon-assisted tunneling
Andreev current
Non-equilibrium quasiparticles and DOS of aluminium superconductor

Realization of unit *ampere* and the quantum triangle experiment

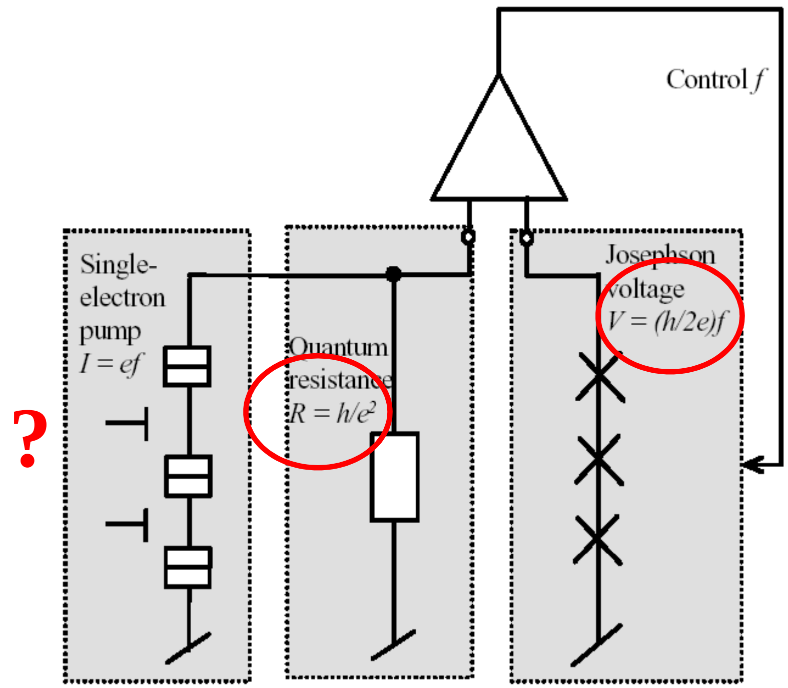

Low temperature laboratory

MIKES Centre for metrology and accreditation

VTT

Requirement: Current > 100 pA with accuracy 10^{-7} ... 10^{-8}

N. Feltin and F. Piquemal, Eur. Phys. J. Spec. Top. 172, 267 (2009).

Single-electron transistor

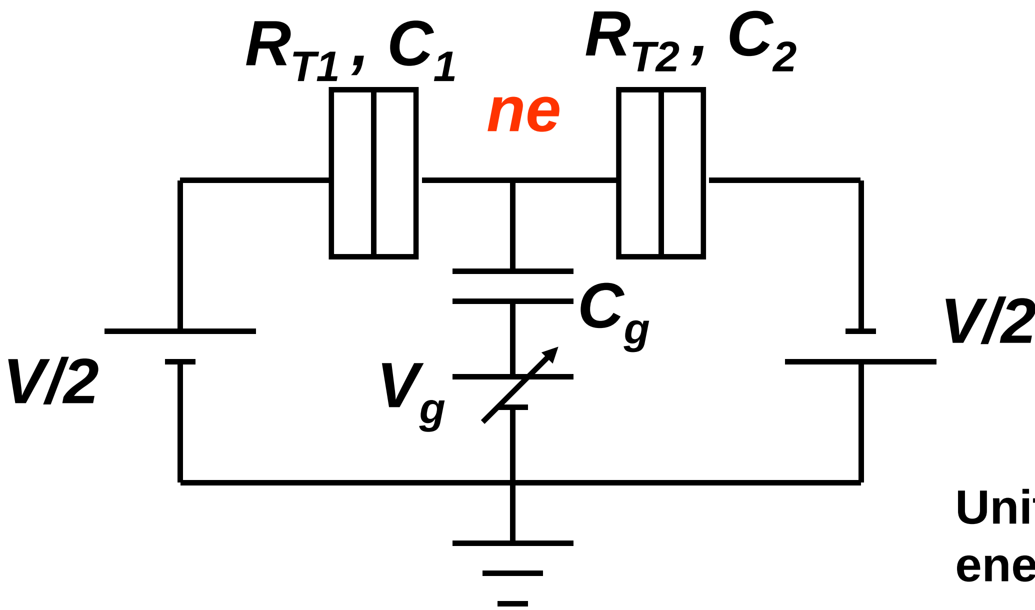

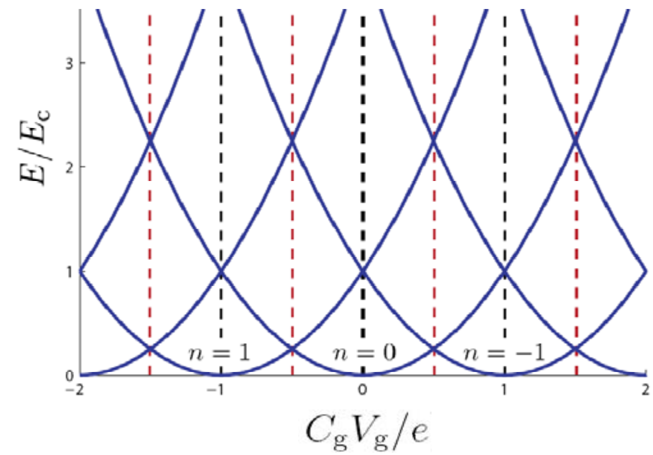

Unit of charging energy: $$E_C = \frac{e^2}{2C_\Sigma}$$

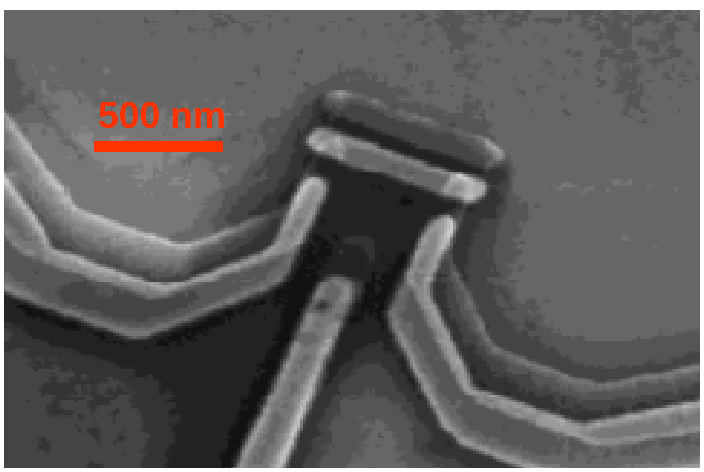

Normal state SET

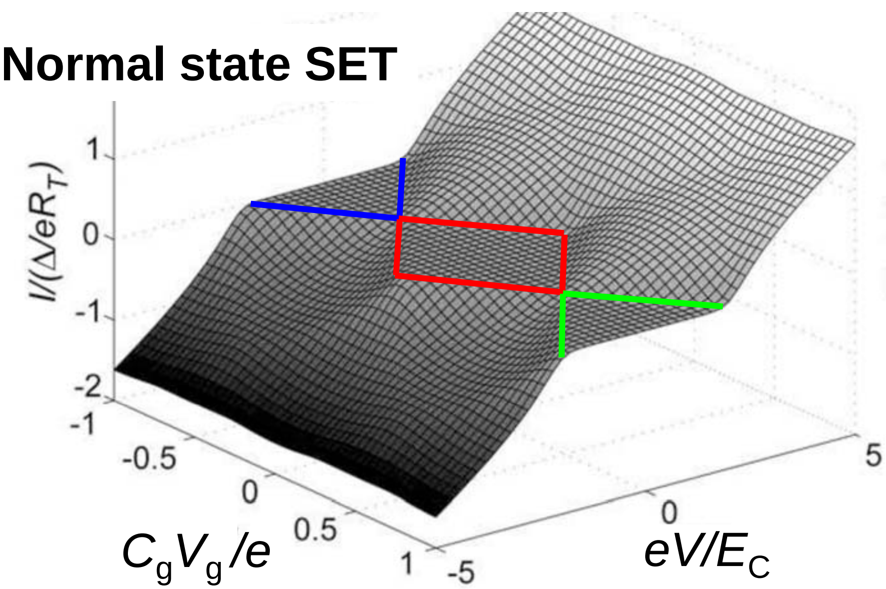

Charge pumps: general principle

Cyclic operation (frequency *f*) of gates, $q_i = C_{gi}V_{gi}/e$, transports charge through the system

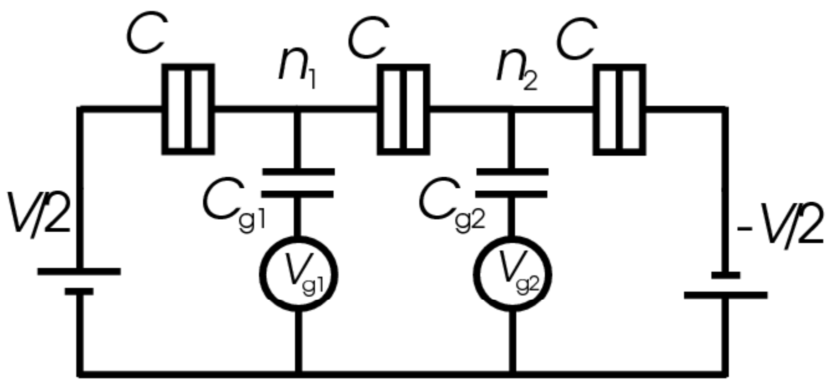

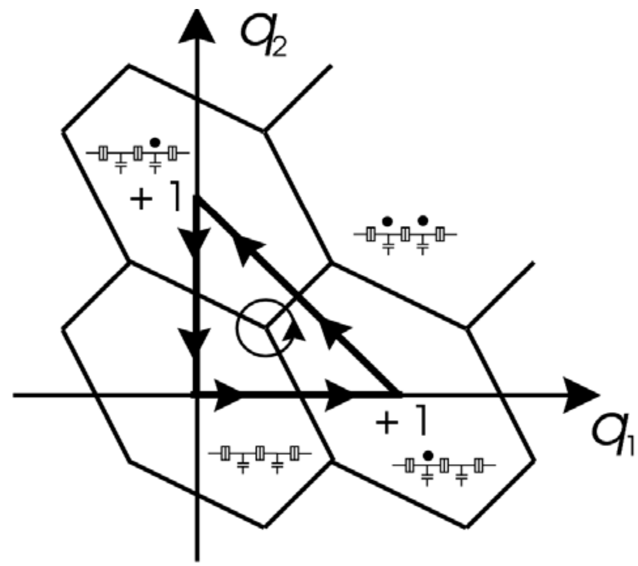

$I = ef$

H. Pothier et al., EPL 17, 249 (1992)

Single electron sources

Towards frequency-to-current conversion

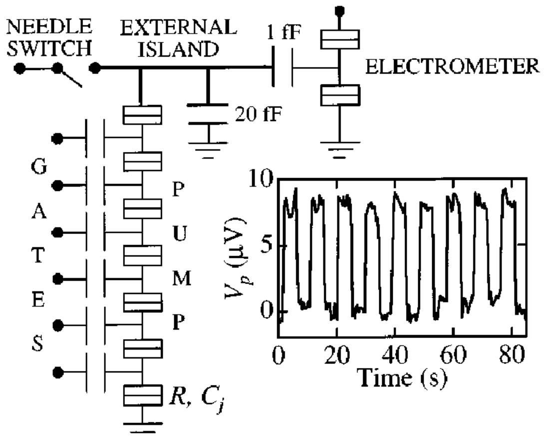

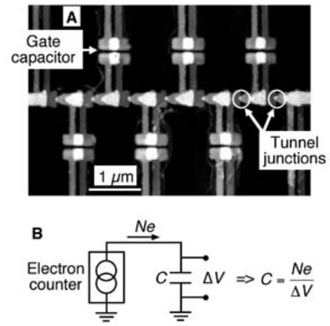

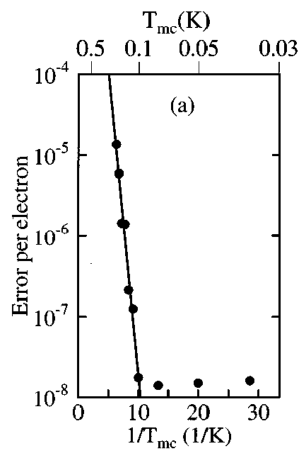

Semiconductor devices, travelling wave or quantum dots:

Shilton et al. 1996

Fujiwara et al. 2004

Blumenthal et al. 2007

Fève et al., 2007

Kaestner et al. 2007

Giblin et al., 2010

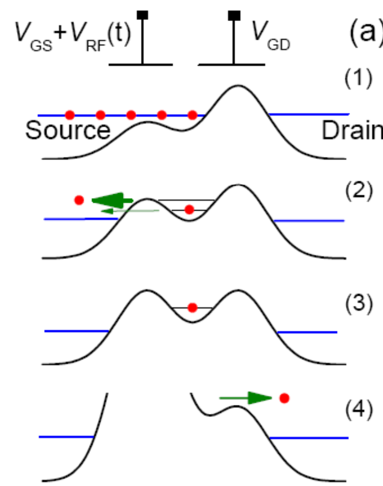

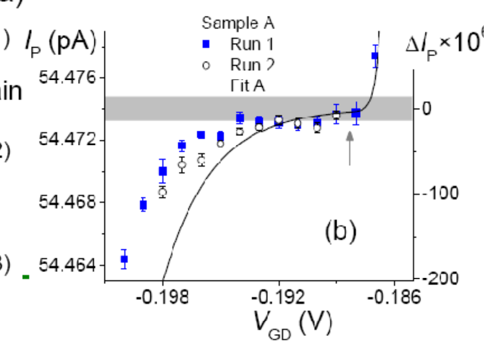

Normal single-electron pump: $\boxed{I = ef}$

Geerligs et al. 1990, Pothier et al. 1992, Keller et al. 1996, Lotkhov et al. 2000

High accuracy but still slow: I << 10 pA

Fully superconducting devices:

Several versions

Fast, but difficult to suppress errors

Mechanical shuttles:

Konig et al. 2008

Single-electron turnstile with NIS-junctions for metrology

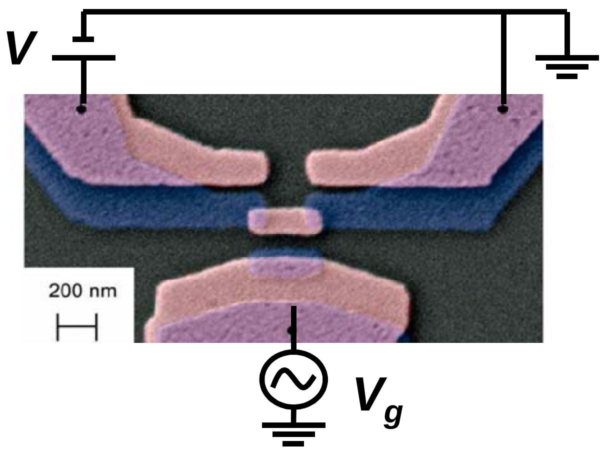

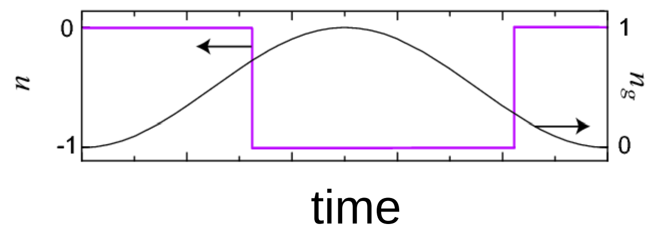

Nature Physics 4, 120 (2008)

One electron is transferred through the turnstile in each gate cycle: *I = ef.*

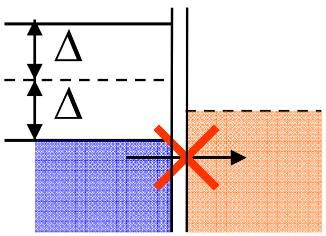

Superconducting gap blocks single-electron tunneling at low energies

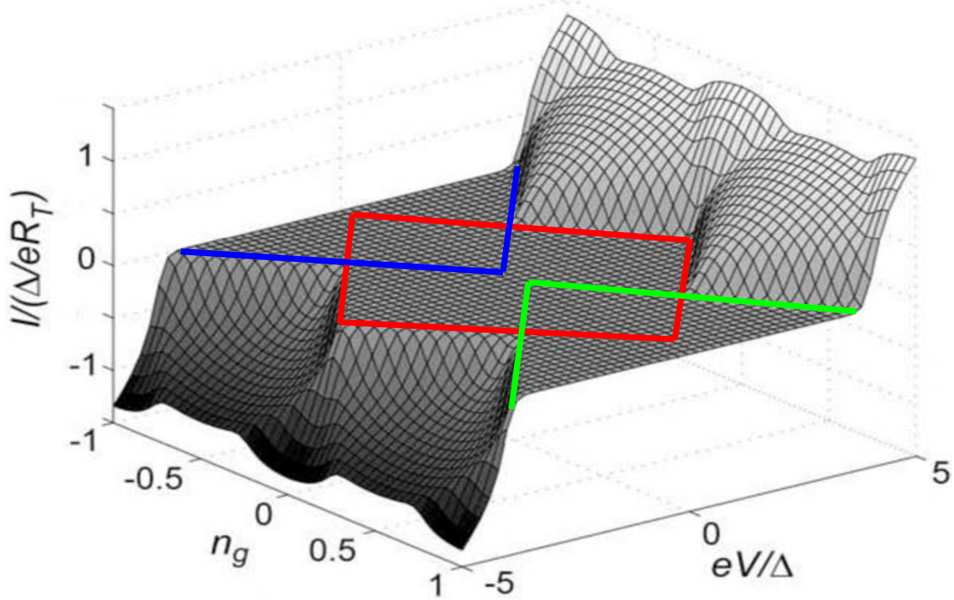

Hybrid single-electron turnstile

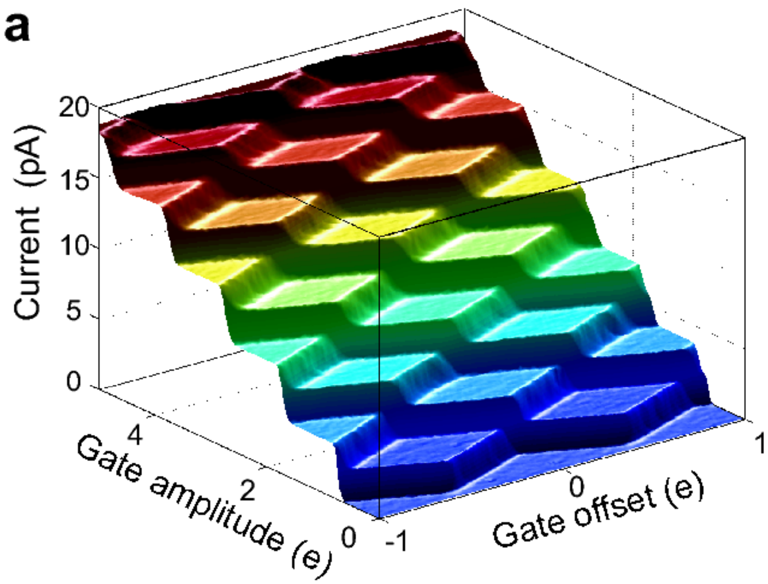

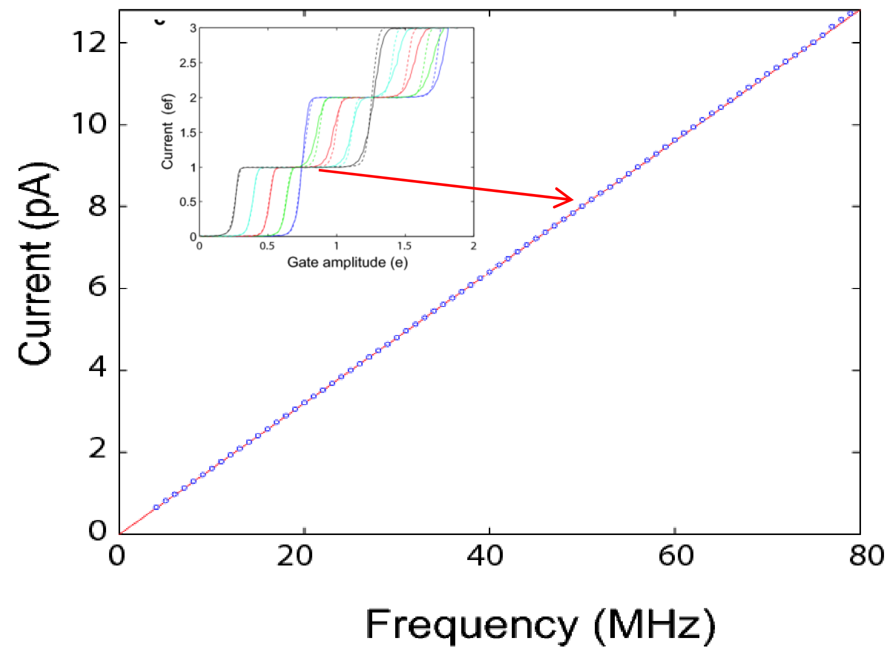

<u>Error sources:</u>

Thermal errors, background charges, errors at high frequencies
Residual and generated quasiparticles in a superconductor
Photon-assisted tunneling
Multi-electron processes (co-tunneling, Andreev tunneling etc.)

Cooper pair – electron cotunnelling (3rd order process)

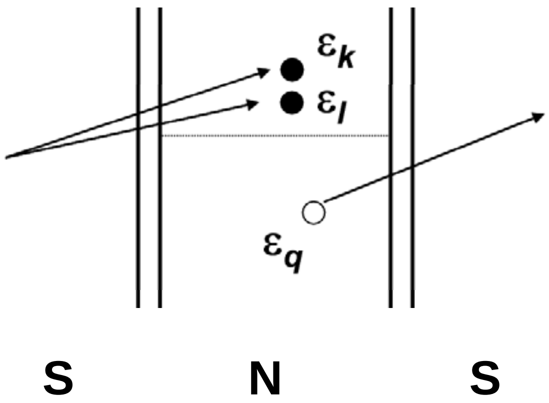

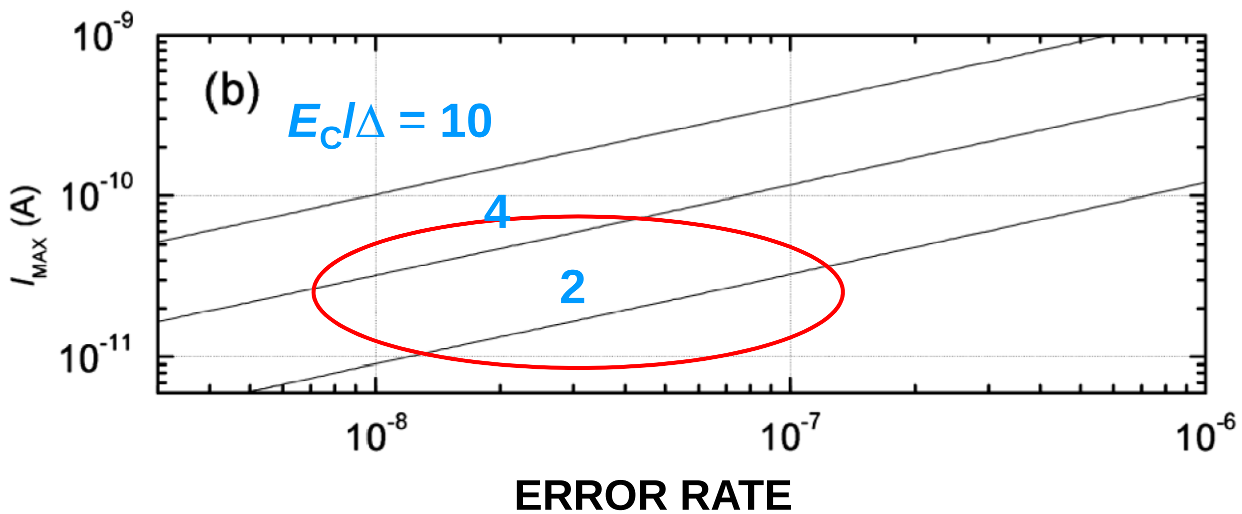

METROLOGICAL REQUIREMENTS ARE IDEALLY SATISFIED IN THEORY, BY USING 10 PARALLEL TURNSTILES

D. Averin and J.P., PRL 101, 066801 (2008)
A. Kemppinen et al., APL 94, 172108 (2009)

Realization of the parallel device

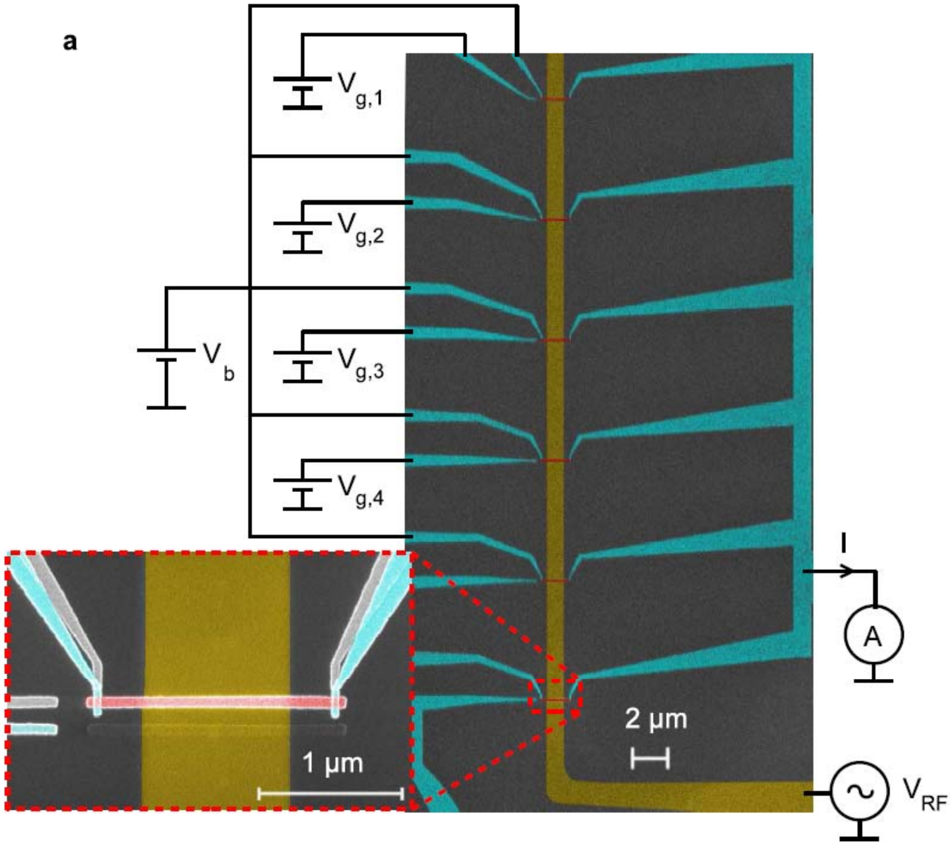

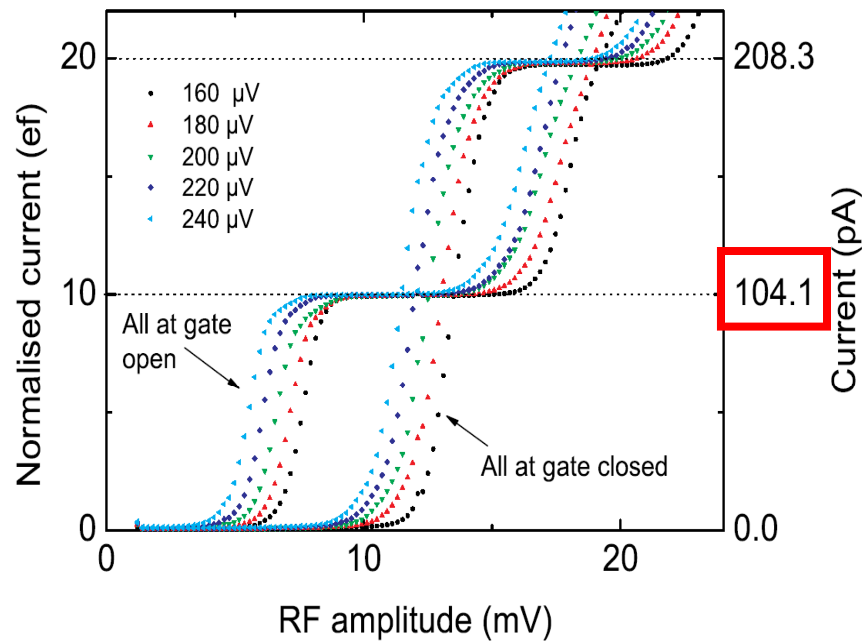

10 PARALLEL TURNSTILES

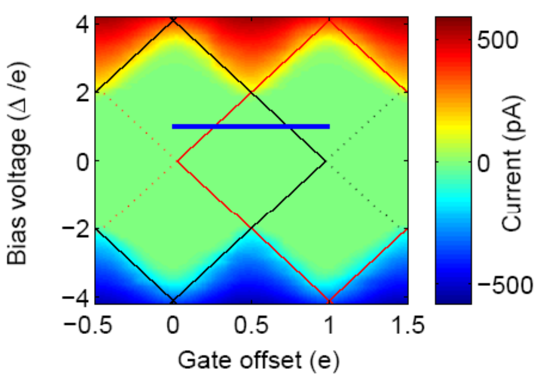

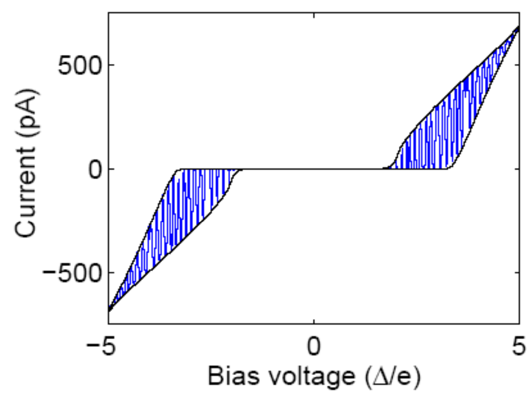

V.F. Maisi et al.,
NJP 11,113057 (2009)

Thermal error rates

Optimum operation point of the turnstile is at $eV = \Delta$, where the error rate is

$$\sim \exp\left(-\frac{\Delta}{k_B T_N}\right)$$

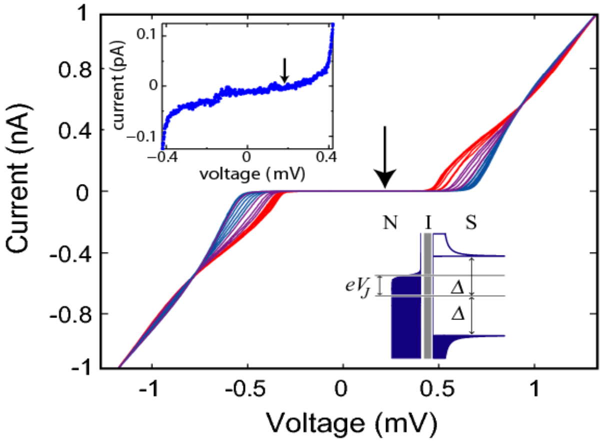

At 100 mK for aluminium ($k_B T_N/\Delta = 0.04$), this error is $<< 10^{-8}$.

Yet the errors in the first experiments were much higher.

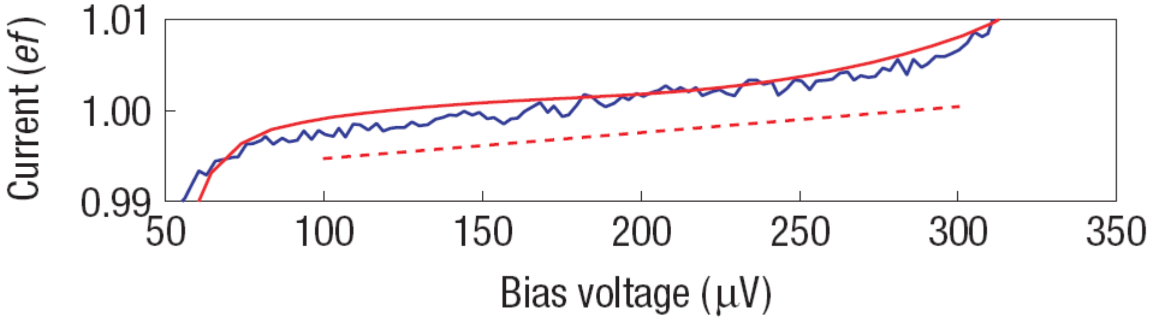

Dynes Density of States

$$n_S(E) = |\mathrm{Re}\frac{E/\Delta + i\gamma}{\sqrt{(E/\Delta + i\gamma)^2 - 1}}|$$

Dynes 1978, 1984

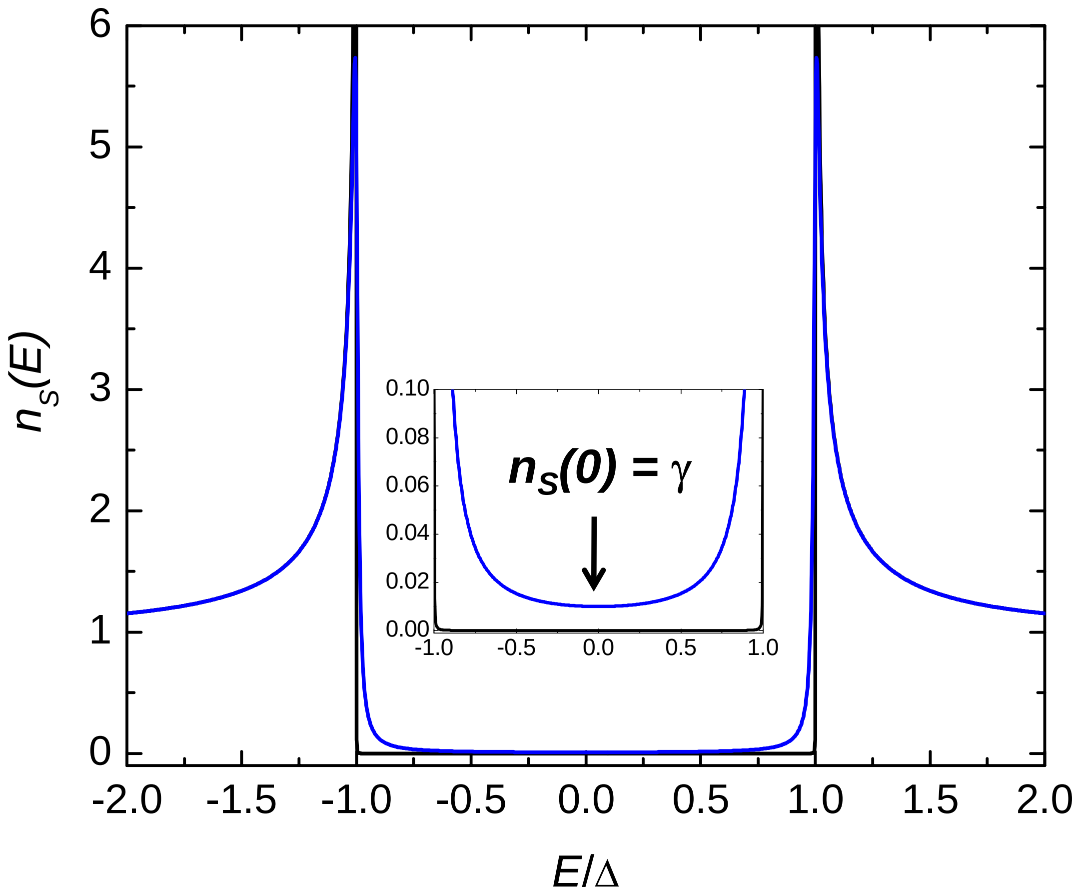

Influence of em-environment on single-electron current in a NIS-junction

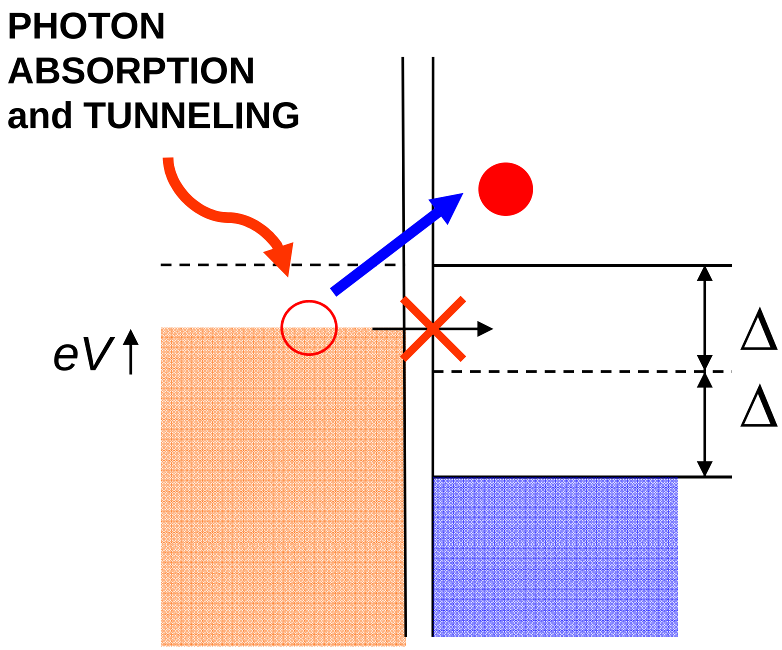

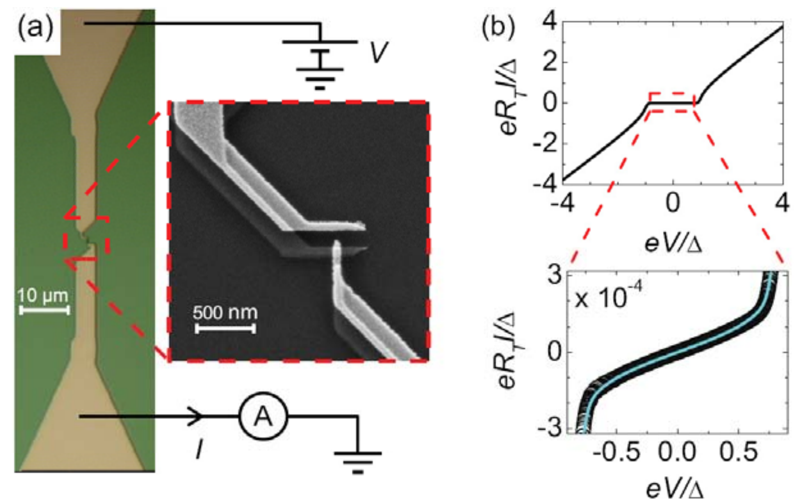

$$I(V) = \frac{1}{eR_T}\int_{-\infty}^{\infty} dE\, n_S^{\gamma}(E)\,[f_N(E-eV)-f_S(E)]$$

with

$$n_S^{\gamma}(E) = \left|\mathrm{Re}\frac{E/\Delta + i\gamma}{\sqrt{(E/\Delta+i\gamma)^2-1}}\right|$$

$$\gamma = 2\pi\frac{R}{R_K}\frac{k_B T_{\mathrm{env}}}{\Delta}$$

PRL **105**, 026803 (2010)

Careful filtering and shielding

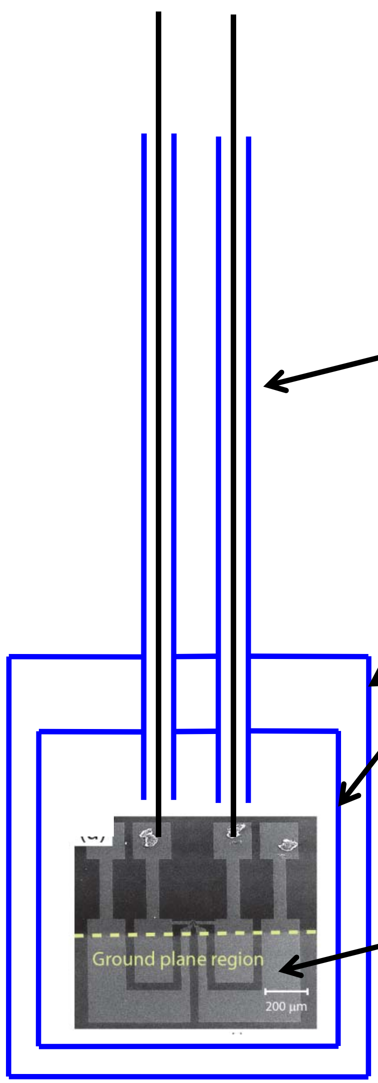

Lossy coaxes with a feed-through

Double-walled hermetic metallic sample stage

On-chip capacitance to shunt the junctions

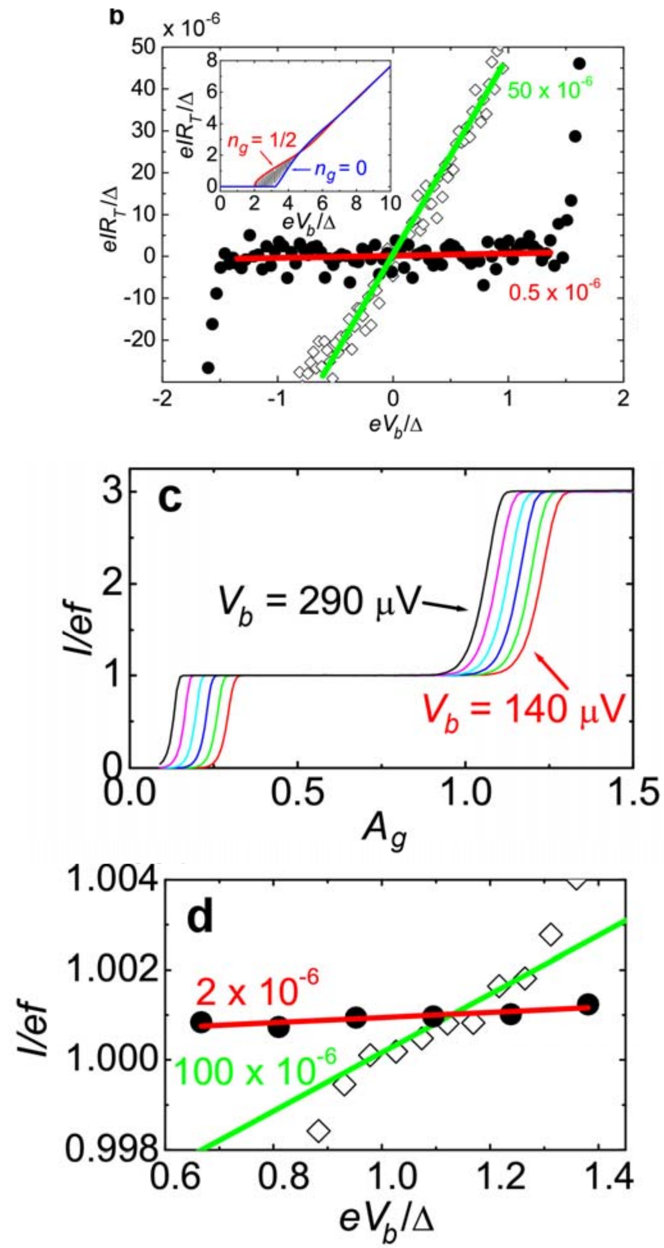

Ultimate error rates – multi-electron processes

COTUNNELLING OF ELECTRONS IN A SINIS STRUCTURE IS EFFICIENTLY SUPPRESSED

”Usual” NININ transistor

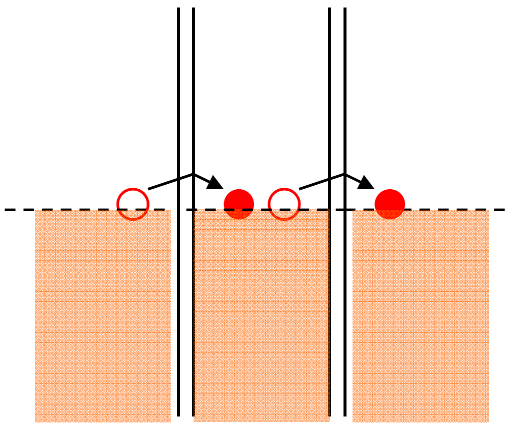

Threshold: $eV = 0$

SINIS transistor

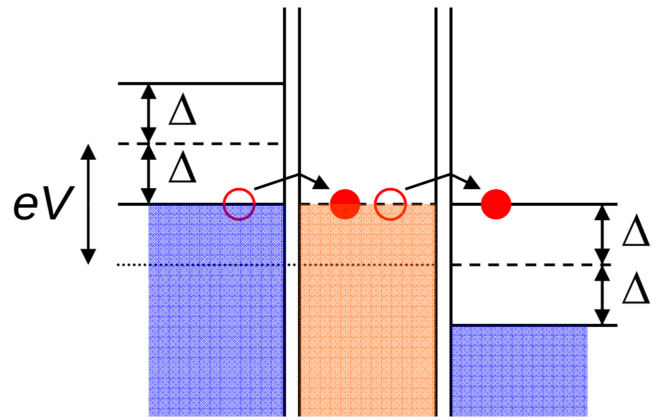

Threshold: $eV = 2\Delta$

NIS junction: 1e vs 2e tunneling

Tunnelling thresholds at T = 0

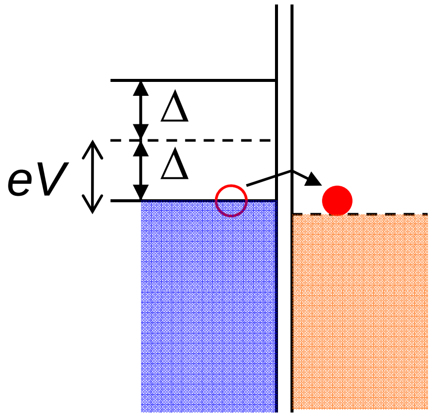

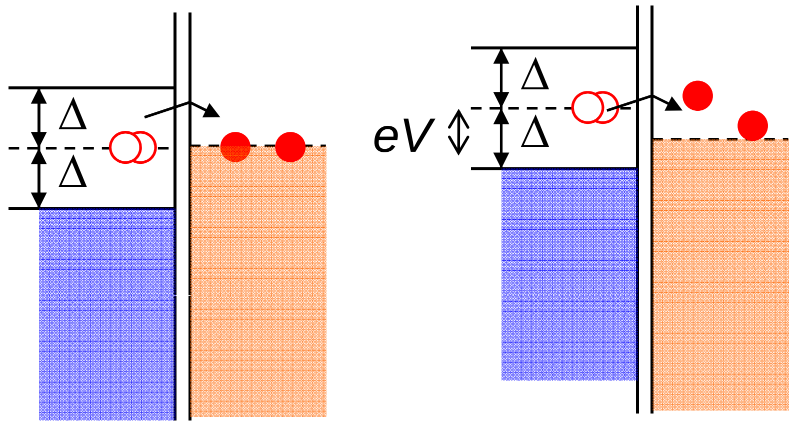

For 1e, threshold at $eV = \Delta$

For Andreev current, no threshold (eV = 0)

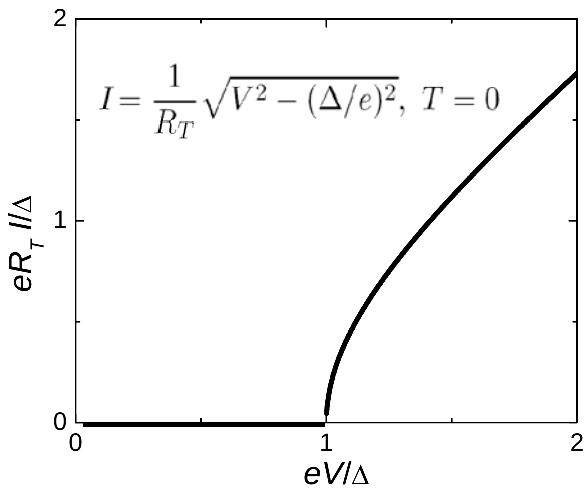

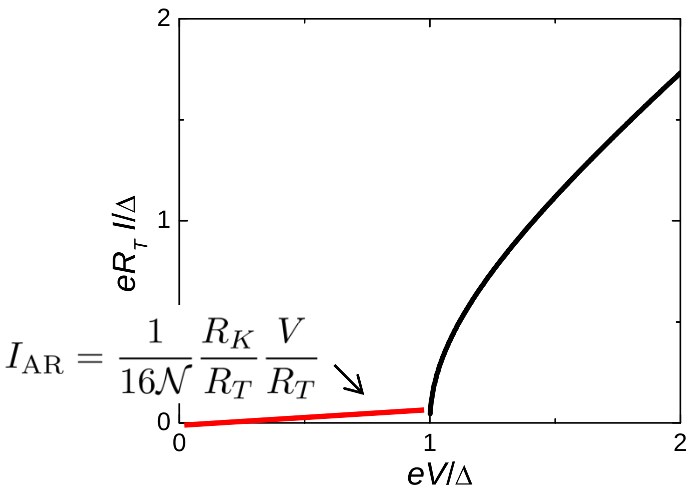

Two-electron current

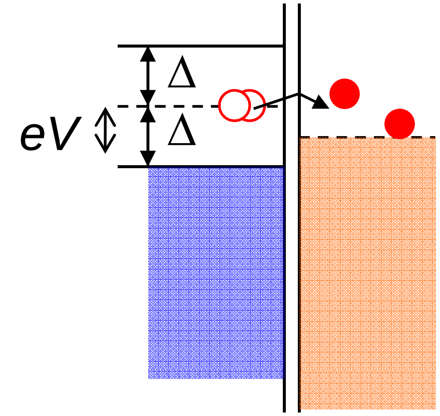

$$A(\epsilon_k, \epsilon_l) = \sum_p u_p v_p t_{pk} t_{pl} \left(\frac{1}{\Omega_p + \epsilon_k - u} + \frac{1}{\Omega_p + \epsilon_l - u} \right)$$

where $u_p, v_p = [(1 \pm \epsilon_p/\Omega_p)/2]^{1/2}$ are the usual BCS quasiparticle factors, $\Omega_p = (\Delta^2 + \epsilon_p^2)^{1/2}$ is the quasiparticle energy, and $u = U^+ + i\gamma(U^+)/2$.

AR rate at $k_B T \ll \Delta$:

$$\gamma_{\mathrm{AR}} = \frac{2\pi}{\hbar} \sum_{k,l} |A|^2 [1 - f(\epsilon_k)][1 - f(\epsilon_l)] \delta(\epsilon_k + \epsilon_l - U^{++})$$

$$\gamma_{\mathrm{AR}} = \frac{\gamma_0 g \Delta}{16\pi \mathcal{N}} \int d\epsilon f(\epsilon - U^{++}/2) f(-\epsilon - U^{++}/2) \times \left| \sum_{\pm} a(\pm\epsilon + E_C - i\gamma/2) \right|^2, \qquad g \equiv \hbar G/e^2.$$

$$a(\epsilon) = (\epsilon^2 - \Delta^2)^{-1/2} \ln \left[\frac{\Delta - \epsilon + (\epsilon^2 - \Delta^2)^{1/2}}{\Delta - \epsilon - (\epsilon^2 - \Delta^2)^{1/2}} \right]$$

Subgap conductance in single NIS junctions – Andreev current(s)

H. Pothier et al., PRL 1994

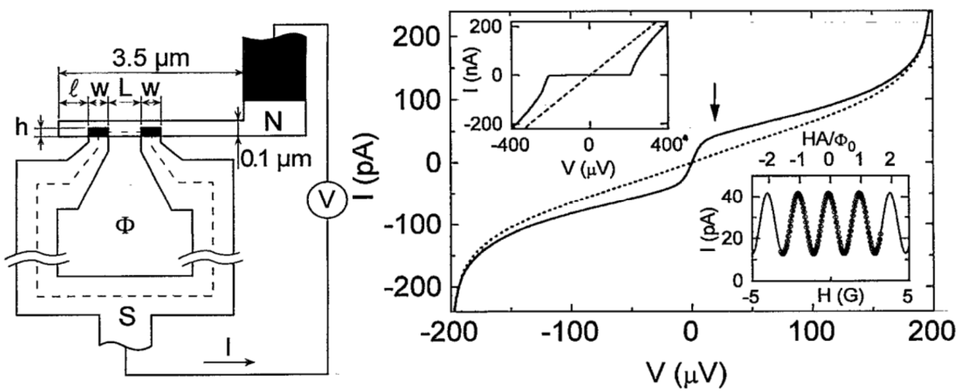

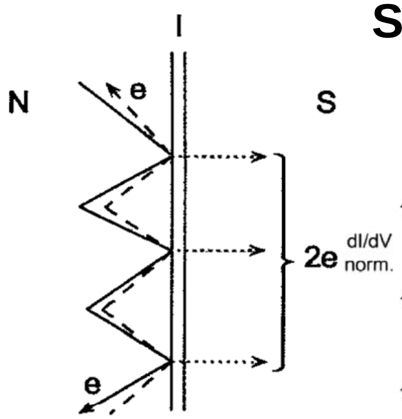

S. Rajauria et al., PRL 2008

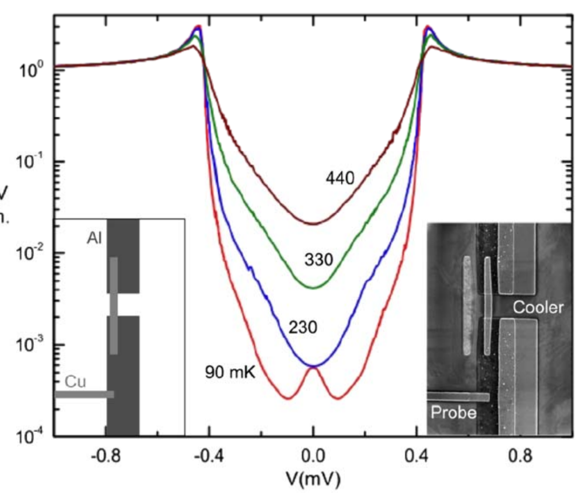

T. Greibe et al., PRL 2011

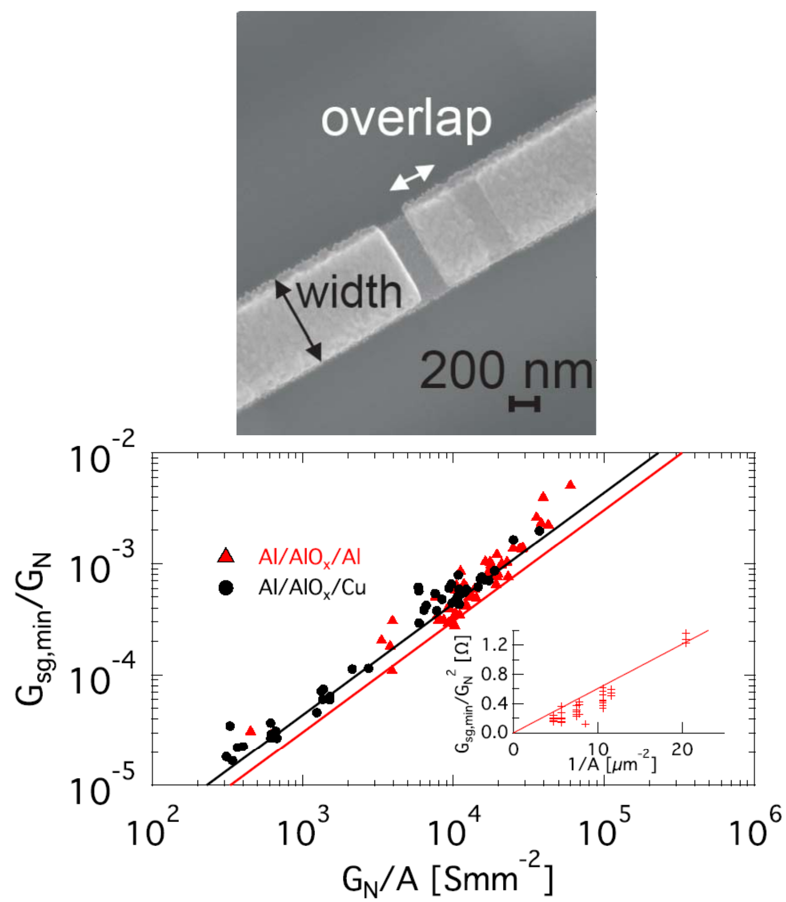

Andreev current in a SINIS SET

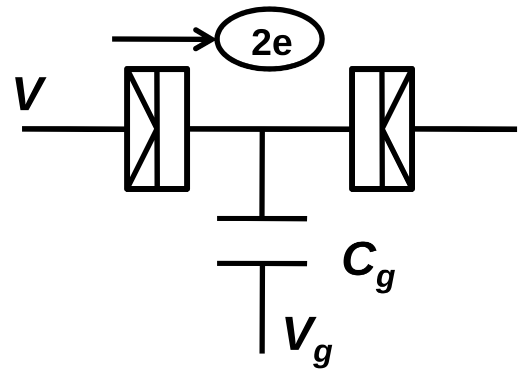

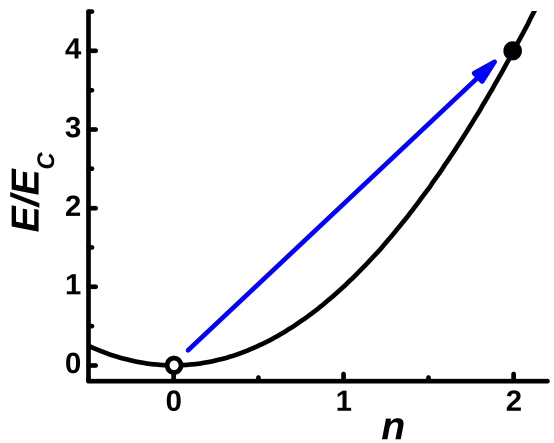

$V_g = 0$.

Tunneling threshold $eV = 4E_C$

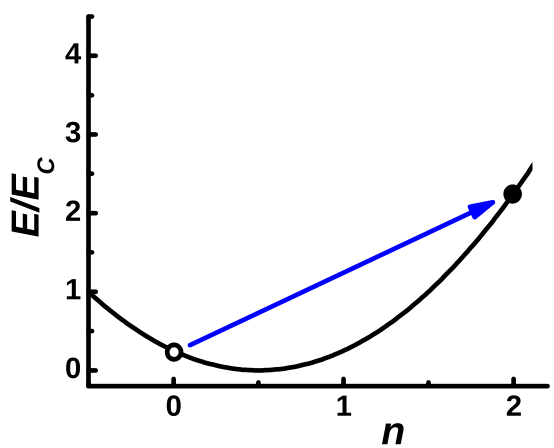

$C_g V_g / e = 1/2$

Tunneling threshold $eV = 2E_C$

Andreev tunneling errors in synchronized electron pumping

Expected single-electron event

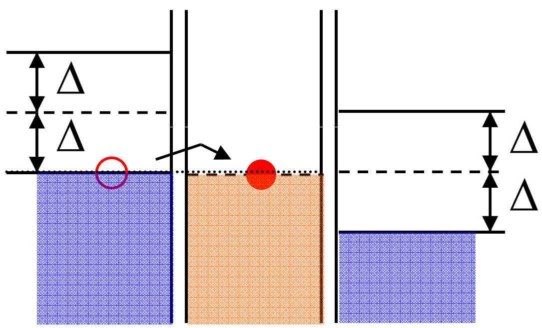

Two-electron tunneling followed by single-electron ejection

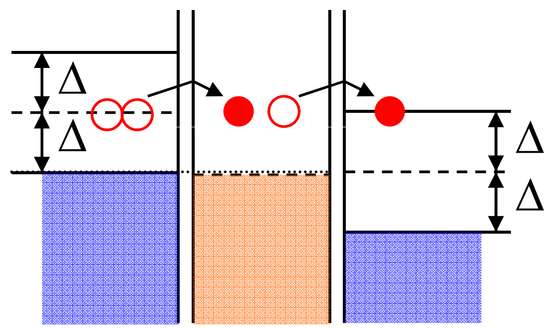

One electron has leaked through

Counting single-electrons

O.-P. Saira et al., PRB 82, 155443 (2010)

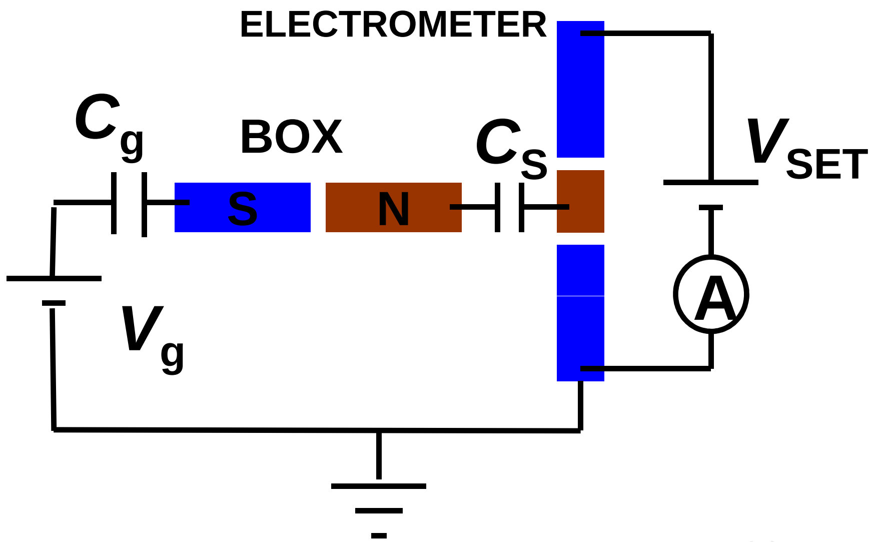

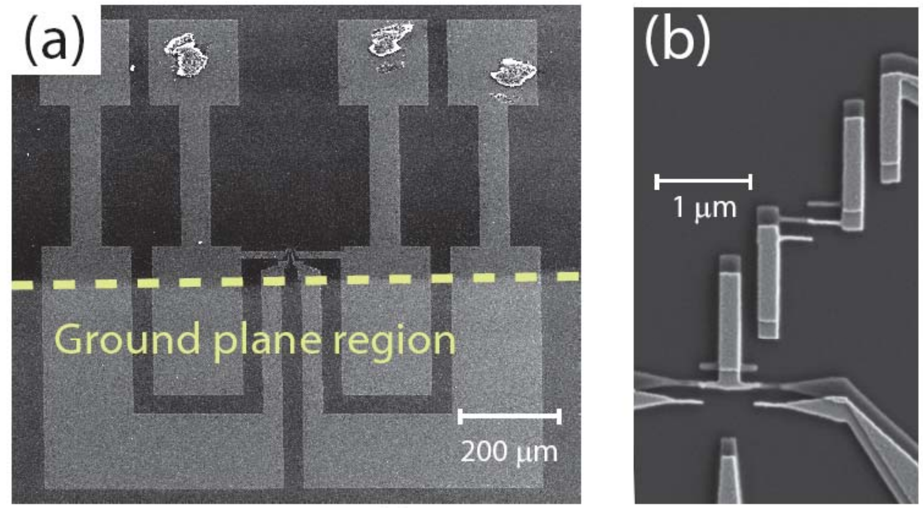

0 – 1 s counting random errors at charge degeneracy
1 – 3 s pumping electrons at 20 Hz frequency
3 – 4 s quiet in the two hold modes

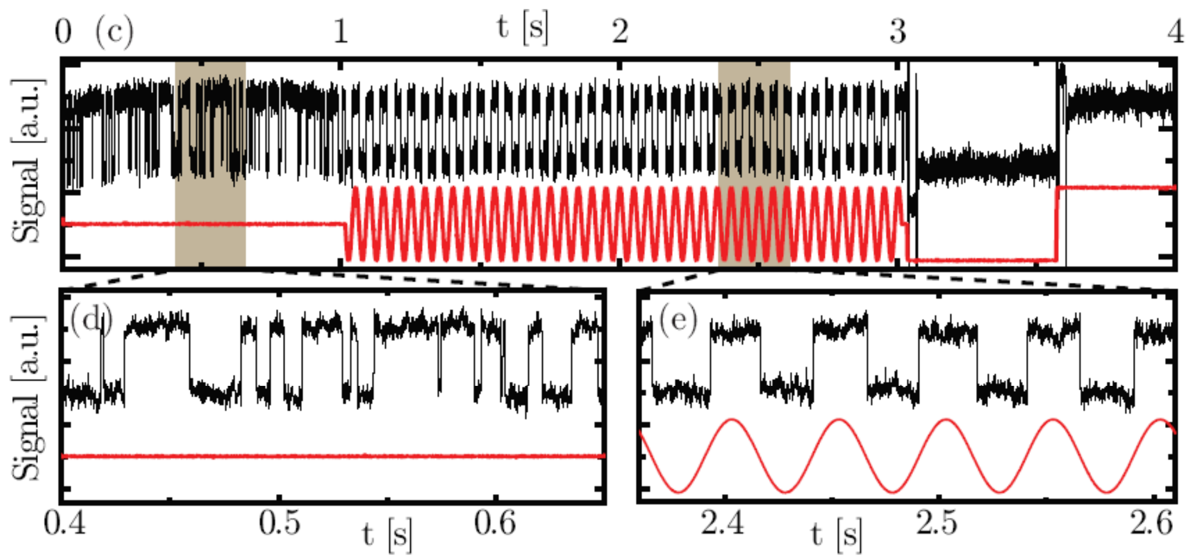

Counting Andreev tunneling events, low E_C box

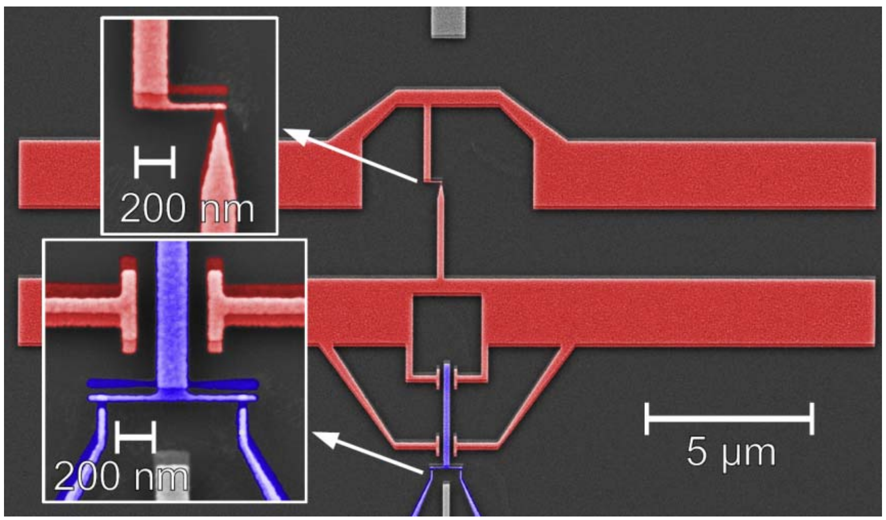

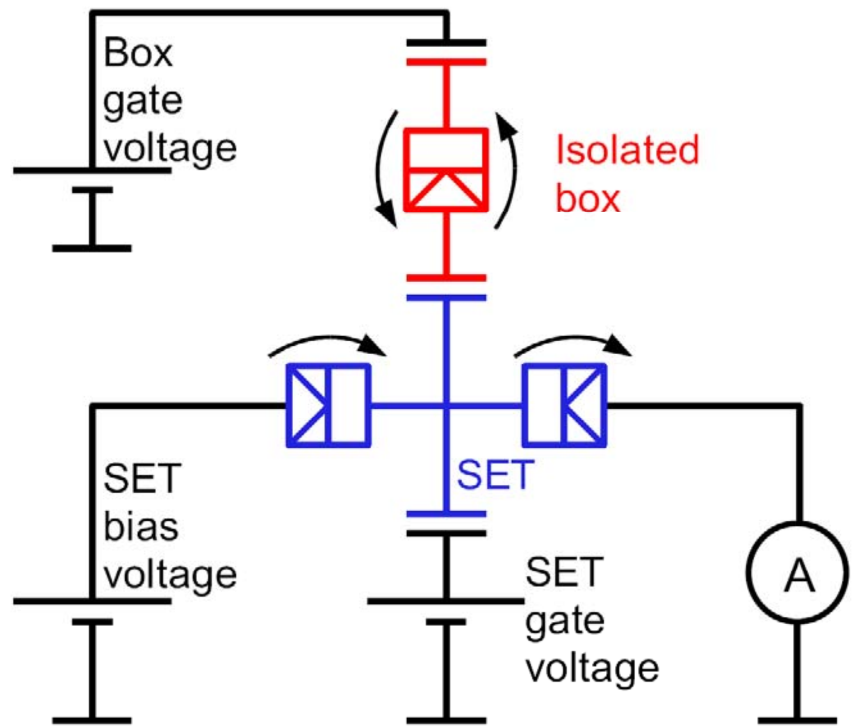

V. Maisi et al., PRL 106, 217003 (2011)

Measured time traces at different gate positions

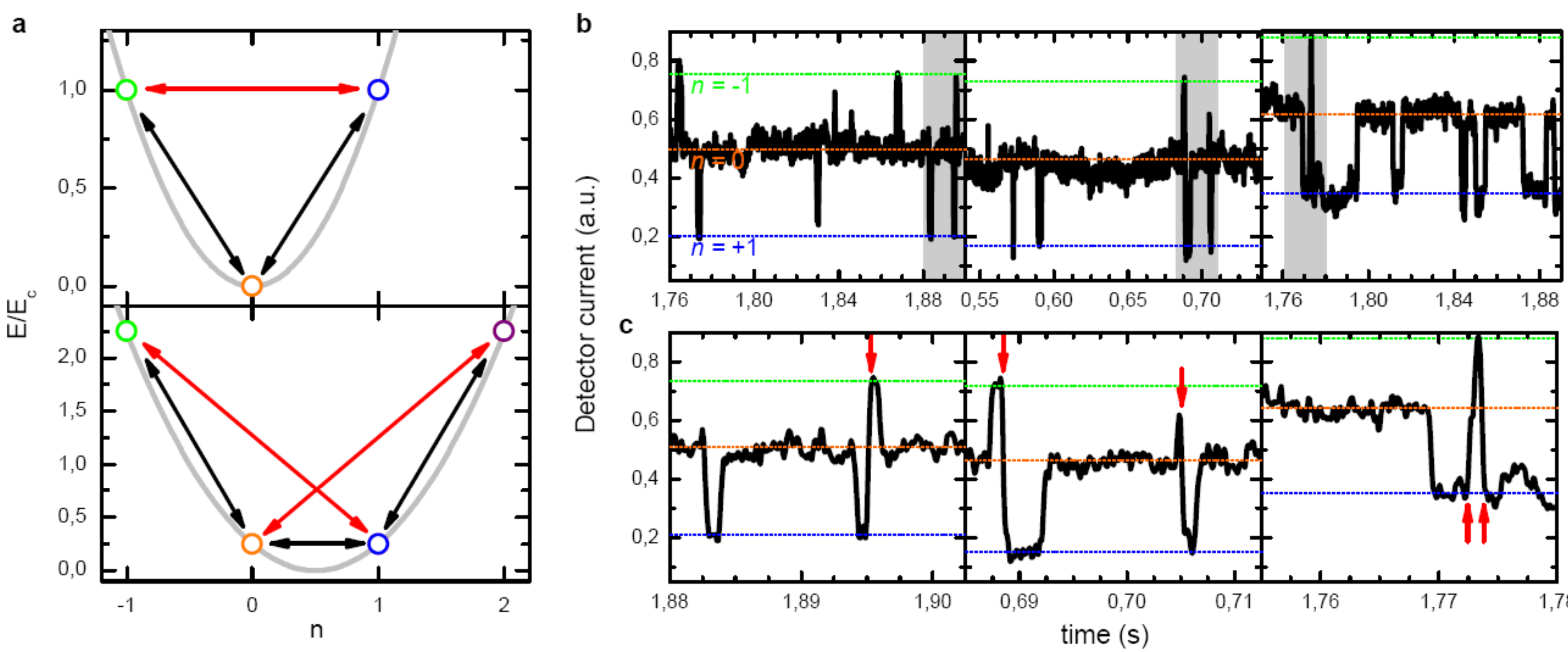

Several 2*e*-like transitions observed

Analysis of the time traces

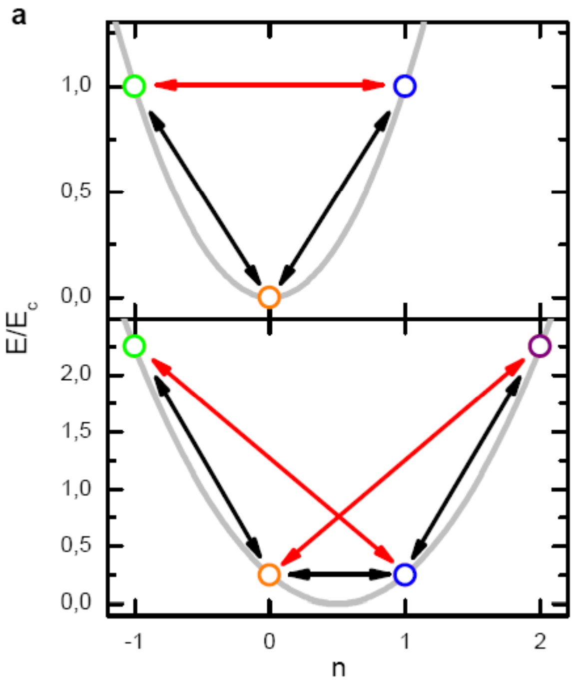

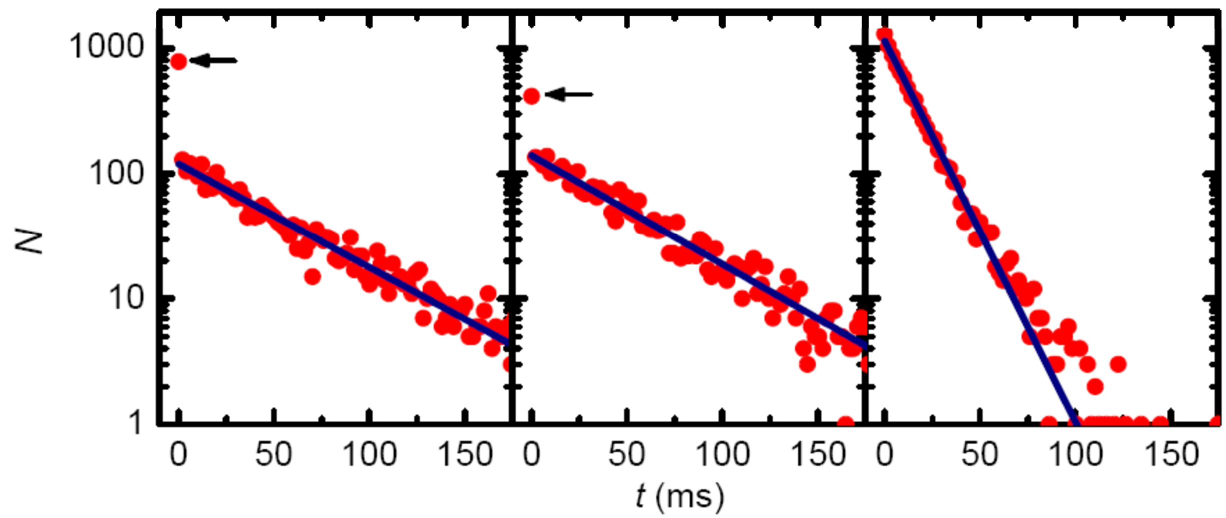

Green lines:

$$\gamma_{\mathrm{AR}} = \frac{\gamma_0 g \Delta}{16\pi\mathcal{N}} \int d\epsilon f(\epsilon - U^{++}/2) f(-\epsilon - U^{++}/2) \times \left| \sum_{\pm} a(\pm\epsilon + E_C - i\gamma/2) \right|^2$$

$$a(\epsilon) = (\epsilon^2 - \Delta^2)^{-1/2} \ln\left[\frac{\Delta - \epsilon + (\epsilon^2 - \Delta^2)^{1/2}}{\Delta - \epsilon - (\epsilon^2 - \Delta^2)^{1/2}}\right]$$

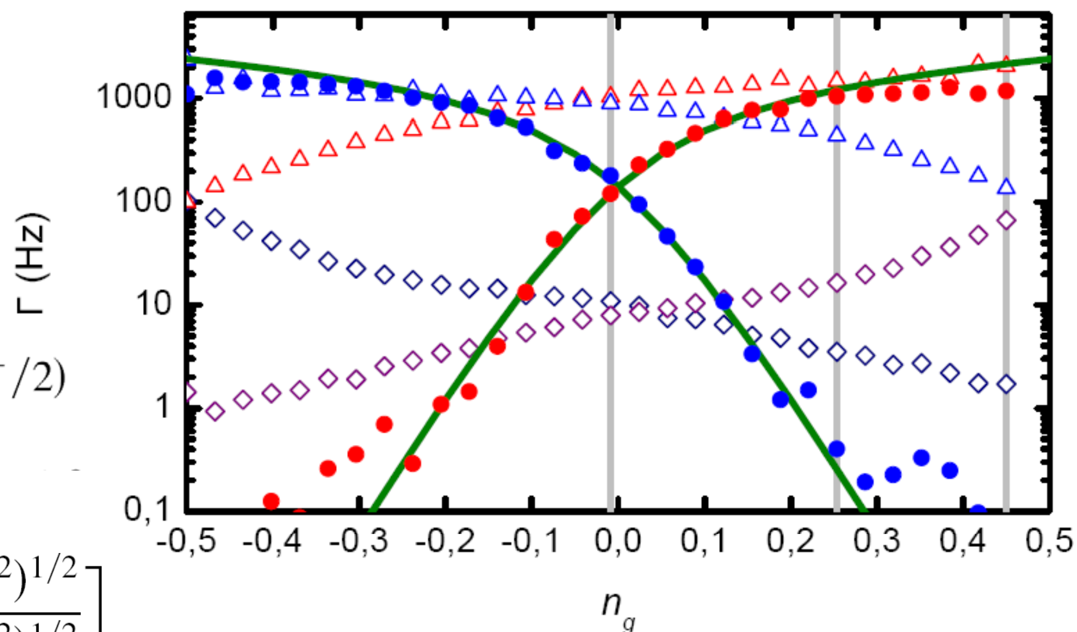

Three experiments on Andreev current

Counting

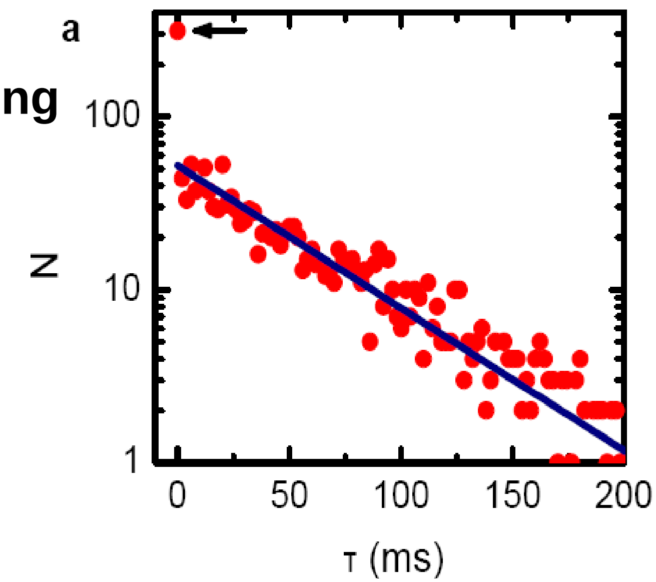

DC-current through an SET

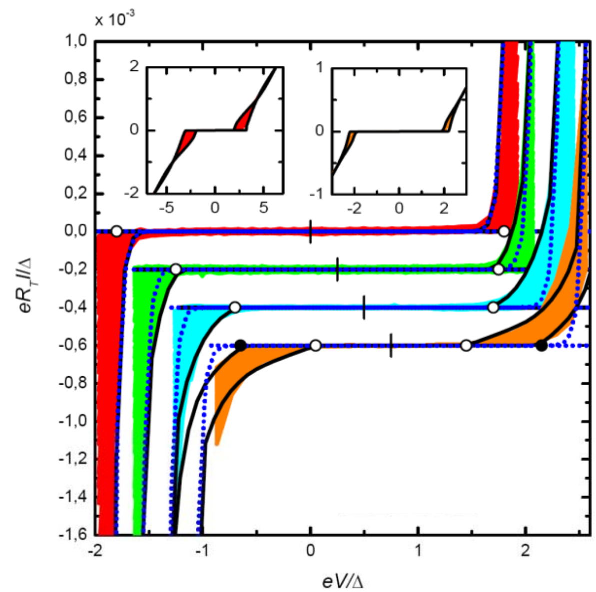

Pumping plateaus of low E_C turnstiles

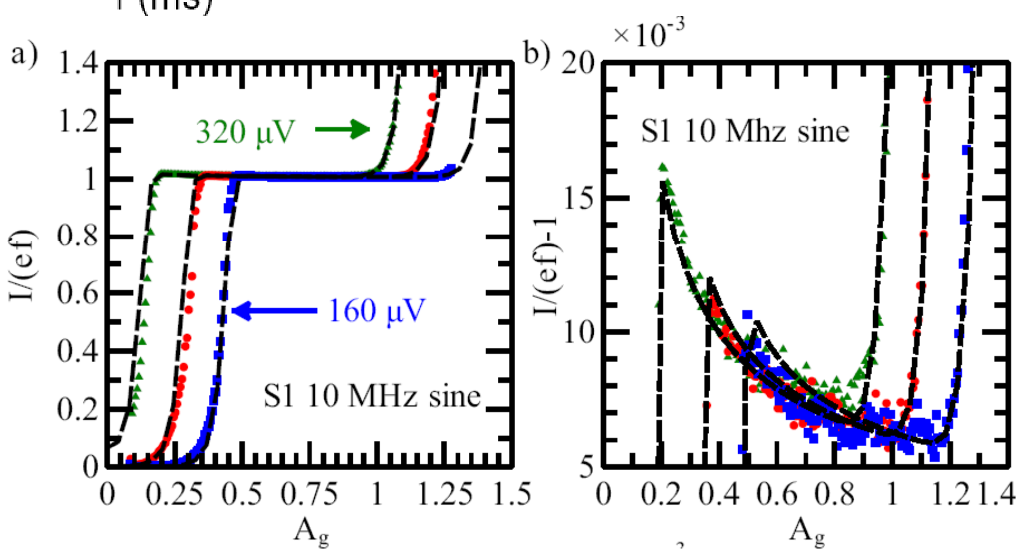

T. Aref, V. Maisi, M. Gustafsson, P. Delsing and J.Pekola, arXiv: 1106.3918, EPL 2011

Consistent results from the three experiments: $S/\mathcal{N}$ = 30 nm^2

Technical conclusion on AR measurements

The channel size, $S/\mathcal{N}$ = 30 nm^2, obtained from experiments, is about one order of magnitude larger than that from naive estimates: for a uniform rectangular tunnel barrier (height ϕ_0, thickness d) it is 2 nm^2

The turnstile current (at a given accuracy) is for the standard AlOx barriers therefore about three times lower than that estimated for a uniform barrier:

$$I_{\max} = ef = \frac{e\Delta}{\hbar}\frac{2\pi}{\ln(1/p)}[\mathcal{N}p\tilde{\gamma}^3/\tilde{\gamma}_{\mathrm{CPE}}]^{1/2}$$

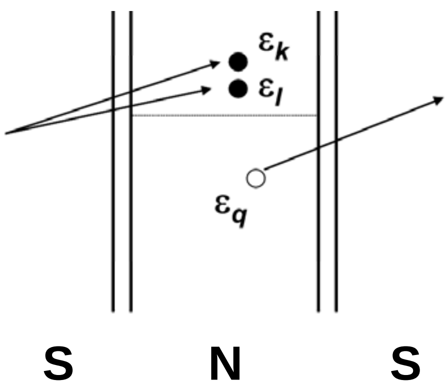

Barrier non-uniformity?

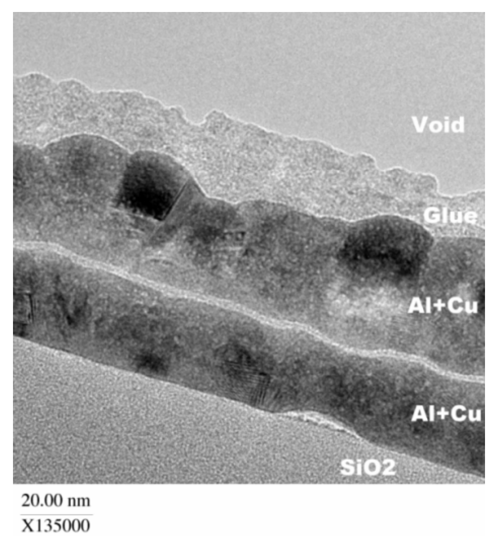

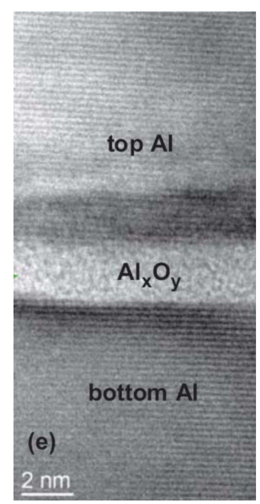

Counting single-electrons on a turnstile

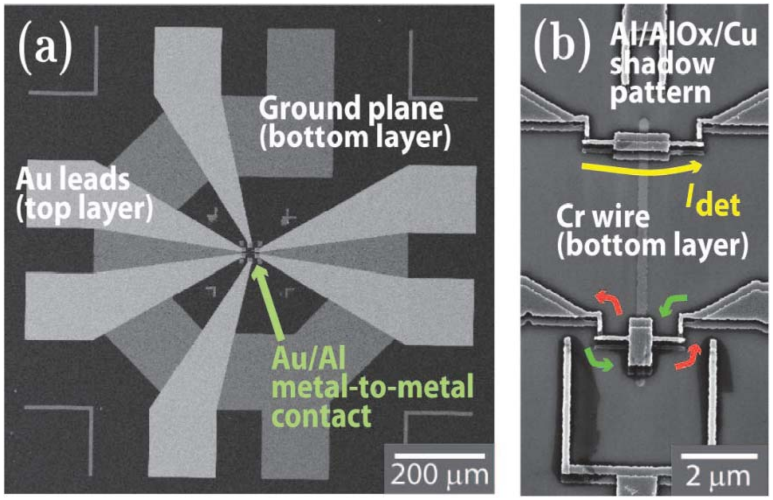

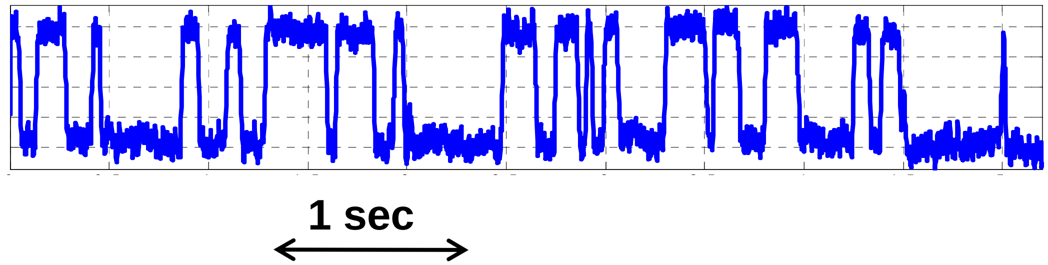

The observed transition rate equals $\Gamma^{1e}(eV_{ds}/2) + \Gamma^{1e}(-eV_{ds}/2)$

The rates can be attributed to:

1. **Residual density of quasiparticles in the superconductor n_{qp}:** $$\Gamma^{1e}_{\mathrm{nqp}} = \frac{n_{\mathrm{qp}}}{2e^2 R_{\mathrm{T}} D(E_F)}$$
2. **Dynes parameter (DOS in the gap) γ:** $\Gamma^{1e}(0) = \gamma \dfrac{k_B T}{e^2 R_T}$

Is Al an ideal superconductor?

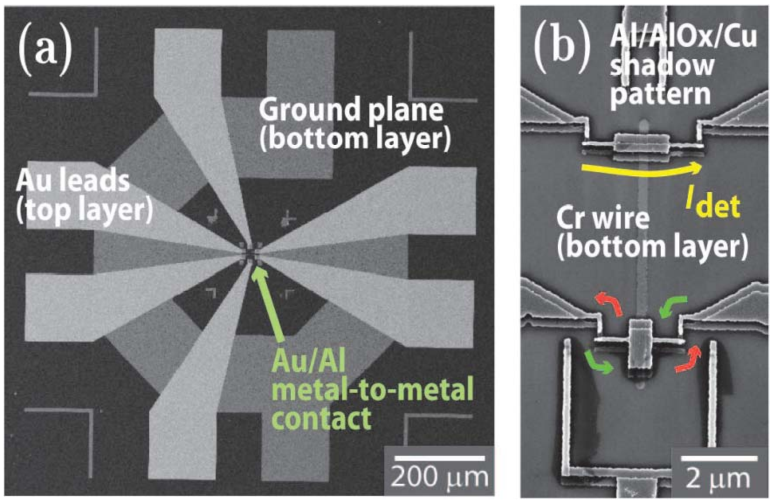

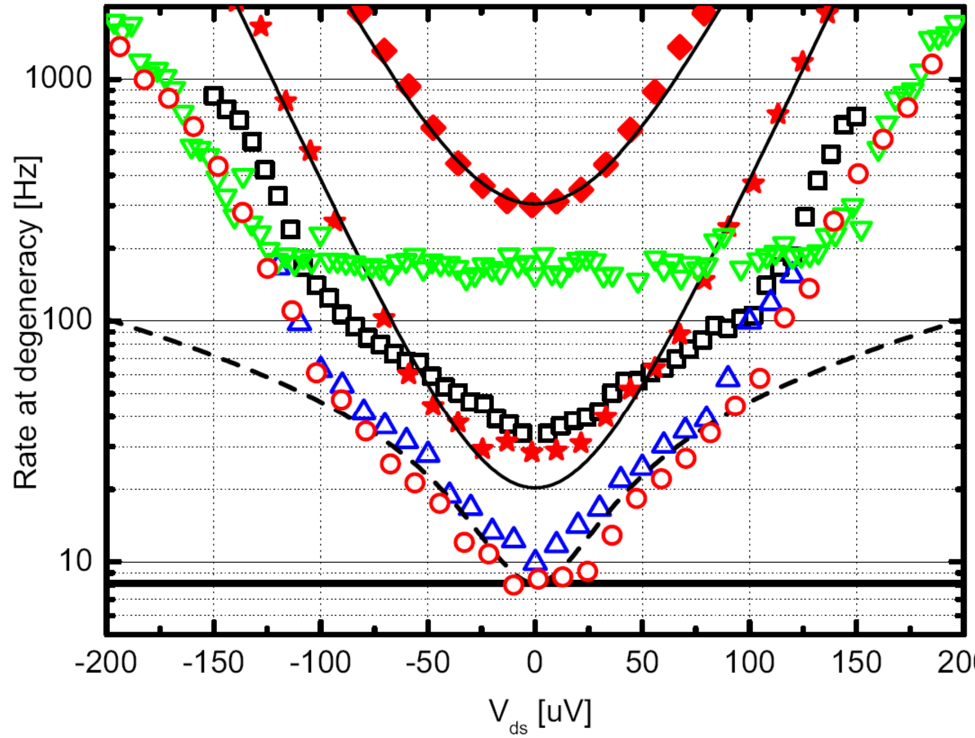

Two major conclusions:

1. Residual quasiparticle density < 0.033 (μm)$^{-3}$:

<u>Typical qp number in the leads = 0</u>

2. Sub-gap density of states < 2 X 10^{-7} $D(E_F)$

O.-P. Saira et al., arXiv:1106.1326

Summary

Photon-assisted tunneling plays a key role

- the device is as good as its environment!

- aluminium is an almost ideal superconductor

Residual quasiparticles need to be controlled

- qp number can be suppressed to <<1

Andreev current was observed in real time and its magnitude was measured quantitatively by three methods:

Subgap current in a SET configuration

Current around the pumping plateau at *$I = ef$*

Direct counting of 2*e* events

SINIS turnstile may eventually qualify for quantum metrology

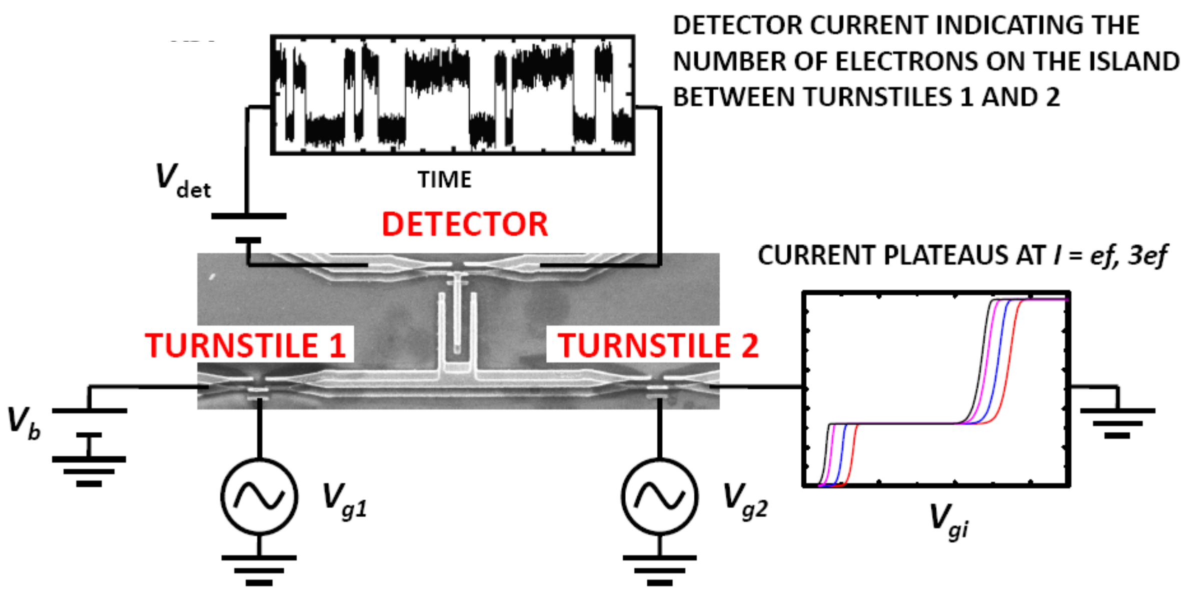

Fluctuation relations (talk tomorrow at Kapitza institute)

Jarzynski equality, C. Jarzynski, PRL 78, 2690 (1997)

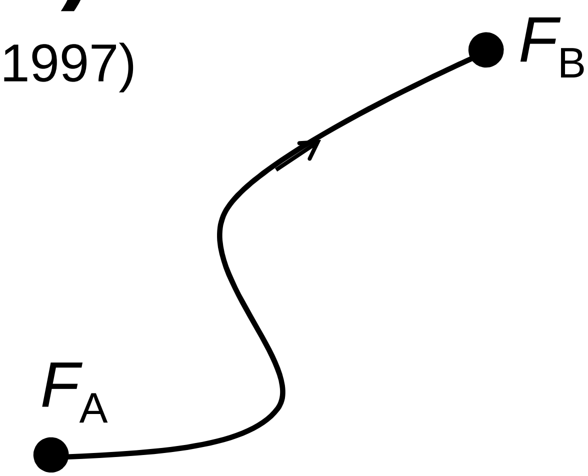

$$\langle e^{-\beta(W-\Delta F)}\rangle = 1$$

This is a powerful expression (equality!):
Since $\langle e^x\rangle \geq e^{\langle x\rangle}$**, we have** $\langle W\rangle \geq \Delta F$ **,**
i.e. 2nd law of thermodynamics.

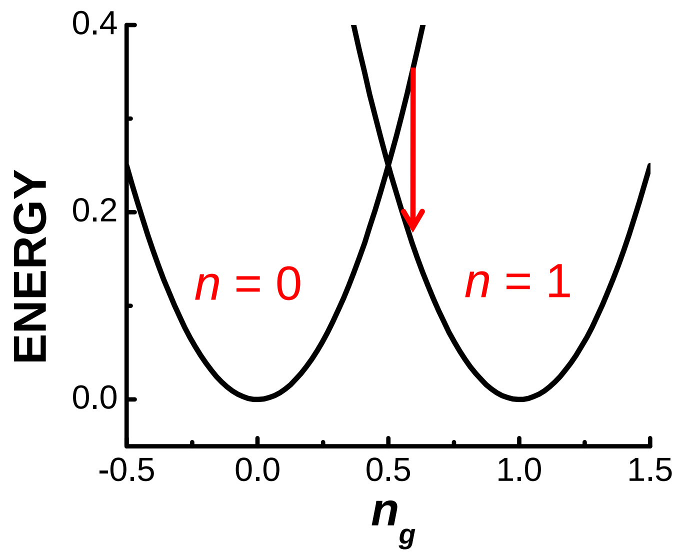

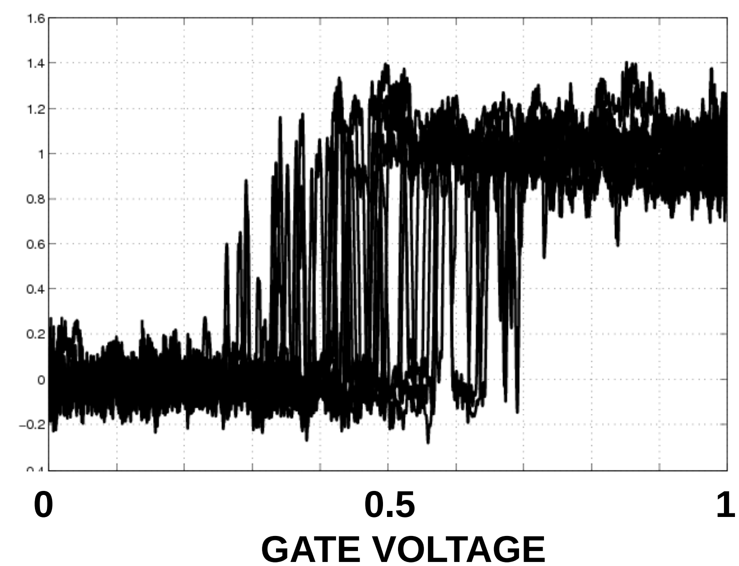

Experimental distributions

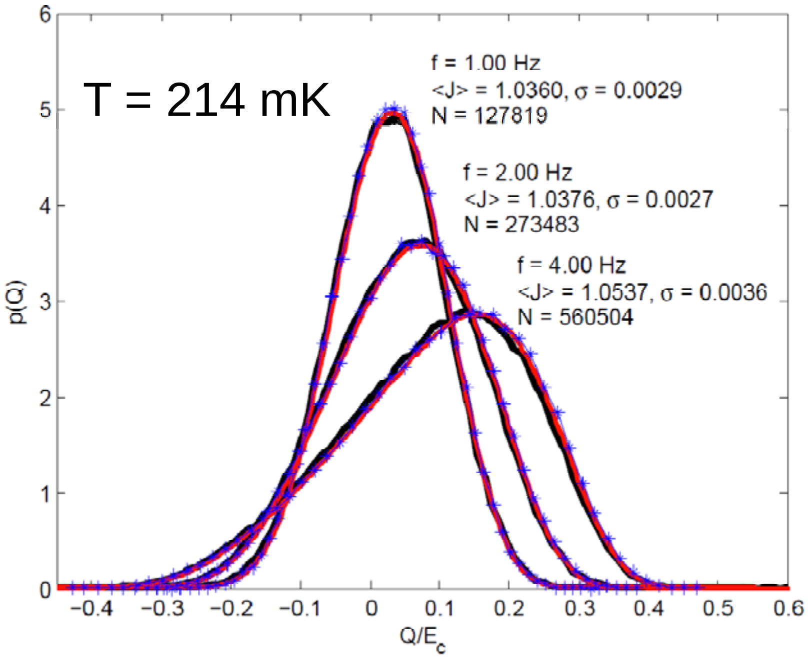

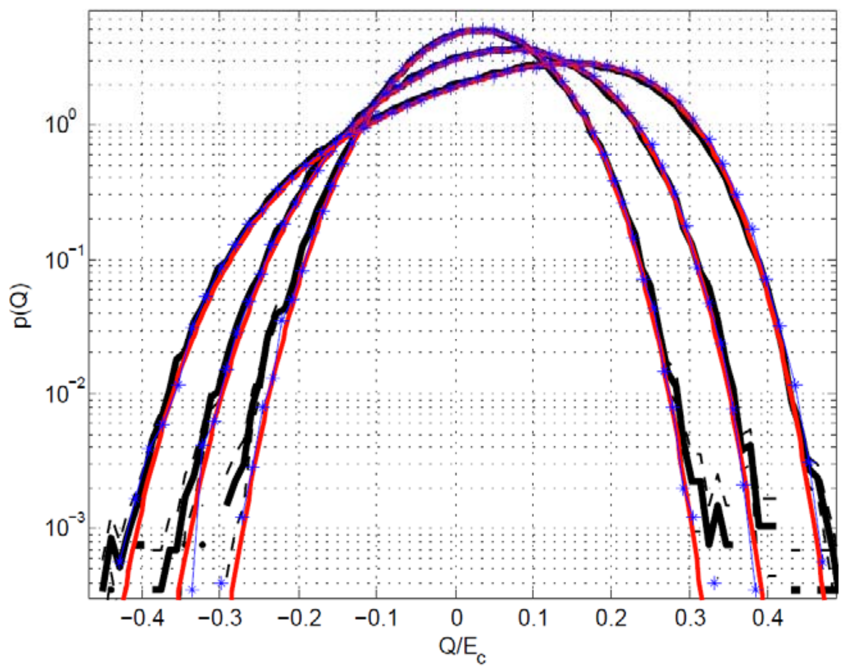

Measured distributions of *Q* at three different ramp frequencies

Taking the finite bandwidth of the detector into account yields

$$\langle e^{-\beta(W-\Delta F)} \rangle = 1 \pm 0.03$$

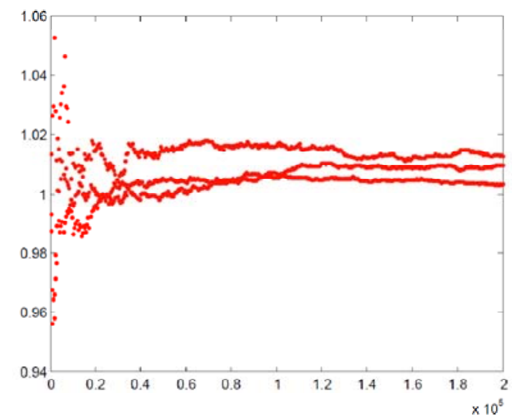

Equilibrium Information from Nonequilibrium Measurements in an Experimental Test of Jarzynski's Equality

Jan Liphardt,[1,4] Sophie Dumont,[2] Steven B. Smith,[3] Ignacio Tinoco Jr.,[1,4] Carlos Bustamante[1,2,3,4]*

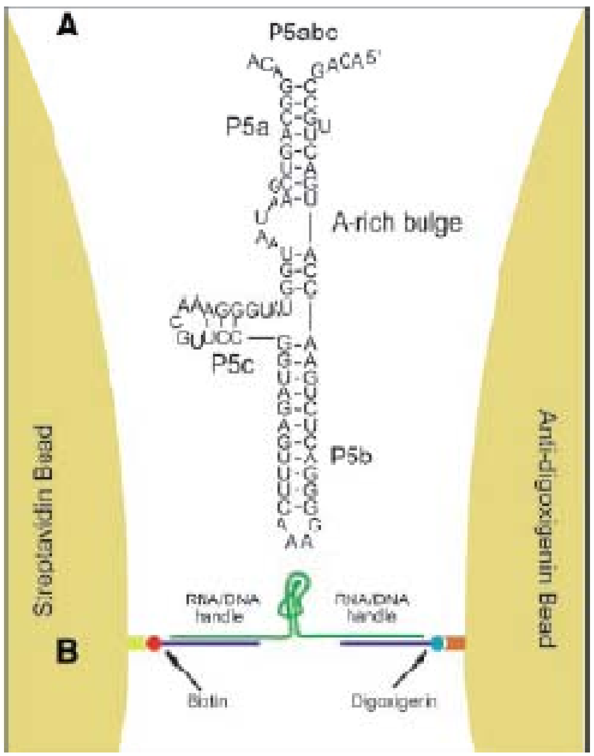

Fig. 1. (A) Sequence and secondary structure of the P5abc RNA. (B) RNA molecules were attached between two beads with RNA-DNA hybrid handles.

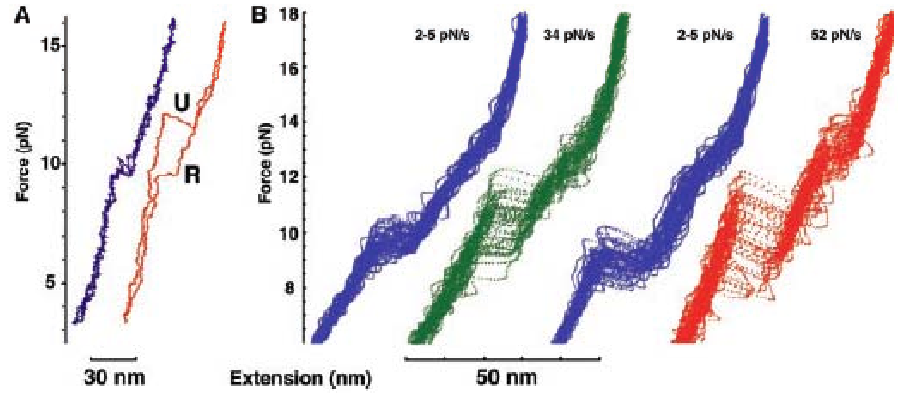

Fig. 2. Force-extension unfolding curves of P5abc at three different switching rates. (A) Typical force-extension unfolding (U) and refolding (R) curves of the P5abc RNA in 10 mM EDTA in reversible (blue, 2 to 5 pN/s) and irreversible (red, 52 pN/s) switching conditions. (B) Two experiments are shown: one in which a molecule was unfolded at rates of 2 to 5 pN/s and 34 pN/s (left pair, blue and green), and another in which the molecule was unfolded at rates of 2 to 5 pN/s and 52 pN/s (right pair, blue and red). Curves (superposition of about 40 curves per experiment) were smoothed by convolution with a Gaussian kernel.

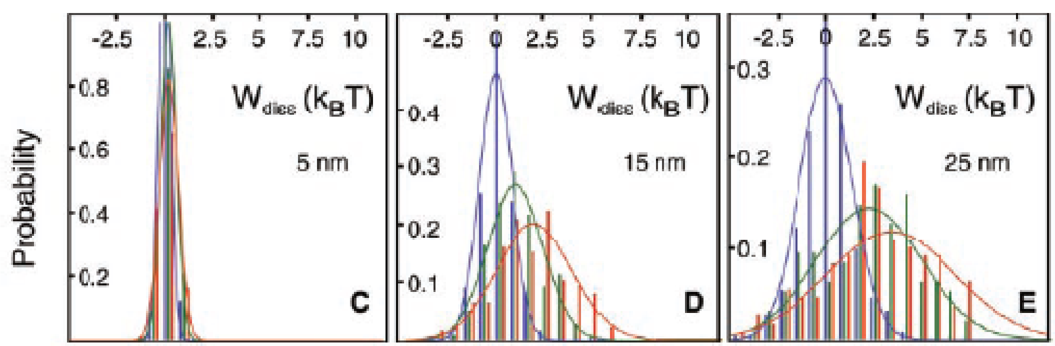

(C to E) Histograms of dissipated work values at z = 5, 15, and 25 nm. Dissipated work values for a given switching rate were pooled. Blue, 272; green, 119; red, 153 dissipated work values. Solid lines: Gaussian with mean and standard deviation of data.

Experimental Free Energy Surface Reconstruction from Single-Molecule Force Spectroscopy using Jarzynski's Equality

Nolan C. Harris, Yang Song, and Ching-Hwa Kiang*

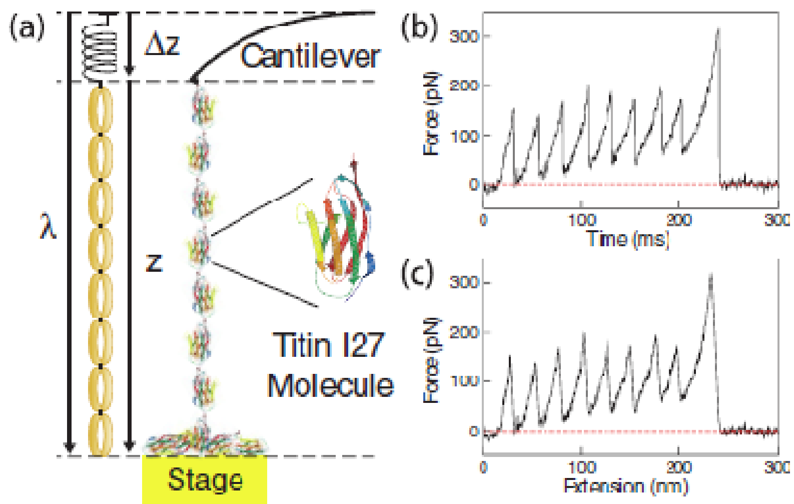

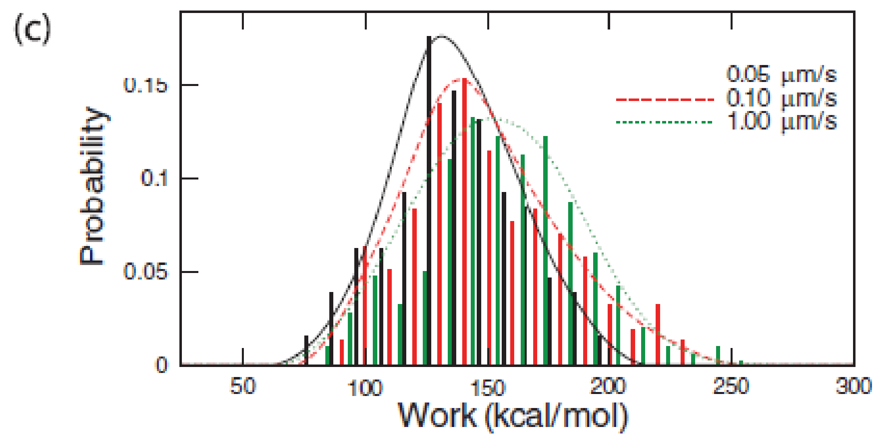

FIG. 1 (color). Single-molecule pulling experiments using AFM. (a) One end of the molecule is attached to the cantilever tip and the other end to a gold substrate, whose position is controlled by a piezoelectric actuator. An analogue of the single-molecule force measurements is illustrated. The cantilever spring obeys Hooke's law, whereas the protein molecular spring follows the wormlike chain model (illustrated using rubber bands).

PAT from detector back-action

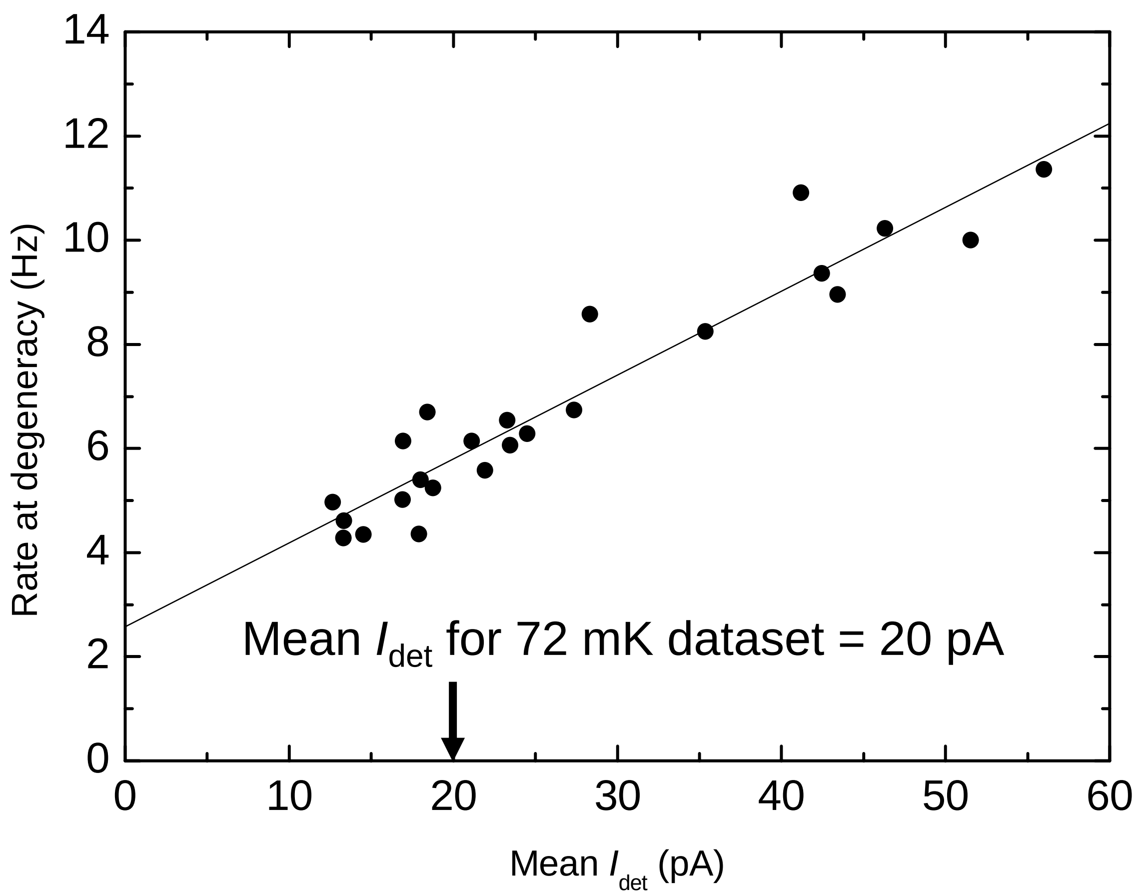

A refined upper bound:

γ **< 1.0 x 10^{-7}**

Aluminium has a very pure BCS gap

Technical conclusions

The channel size, $S/\mathcal{N}$, obtained from both IVG and counting experiments is 30 nm^2, which is about one order of magnitude larger than that from naive estimates: for a uniform rectangular tunnel barrier (height ϕ_0, thickness d) it is 2 nm^2

The turnstile current (at a given accuracy) is for the standard AlOx barriers therefore about three times lower than that estimated before (for a uniform barrier):

$$I_{\max} = ef = \frac{e\Delta}{\hbar}\,\frac{2\pi}{\ln(1/p)}[\mathcal{N}p\tilde{\gamma}^3/\tilde{\gamma}_{\rm CPE}]^{1/2}$$

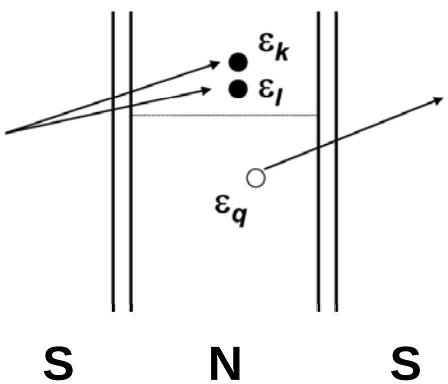

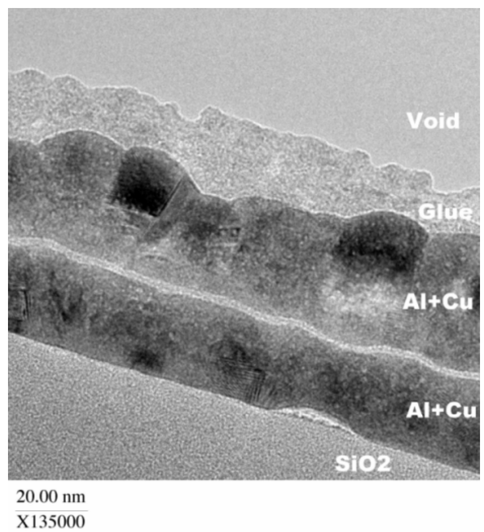

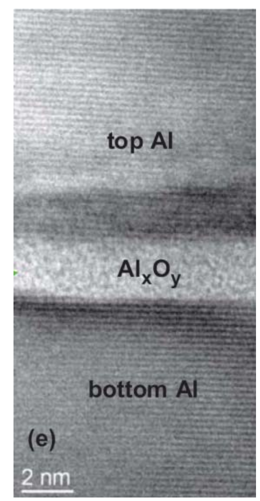

Barrier non-uniformity?

Basic PAT calculations

Relation between PAT and spectral density of voltage fluctuations

$$P(E) = \frac{\pi S_V(|E|/\hbar)}{R_\mathrm{K} E^2}$$

valid for $E < 0$,
S_V sufficiently weak

Detector switching noise is RTN type

$$S_V(f) = \frac{A^2 \tau_c}{1+(\pi f \tau_c)^2}, \text{ where } A = \frac{\kappa e}{C_\Sigma}, \ \tau_c^{-1} = |I_\mathrm{det}|/e$$

- $P(-\Delta) \sim |I_{det}|$ as observed experimentally
- Parameter κ characterizes detector coupling, fit to experimental data gives $\kappa = 0.005$
  - High-frequency back-action filtered by Cr coupling wire

Andreev current and CPE

$$A(\epsilon_k, \epsilon_l) = \sum_p u_p v_p t_{pk} t_{pl} \left(\frac{1}{\Omega_p + \epsilon_k - u} + \frac{1}{\Omega_p + \epsilon_l - u} \right)$$

where $u_p, v_p = [(1 \pm \epsilon_p/\Omega_p)/2]^{1/2}$ are the usual BCS quasiparticle factors, $\Omega_p = (\Delta^2 + \epsilon_p^2)^{1/2}$ is the quasiparticle energy, and $u = U^+ + i\gamma(U^+)/2$.

The amplitude A gives the AR rate at $k_B T \ll \Delta$:

$$\gamma_{\mathrm{AR}} = \frac{2\pi}{\hbar} \sum_{k,l} |A|^2 [1 - f(\epsilon_k)][1 - f(\epsilon_l)] \delta(\epsilon_k + \epsilon_l - U^{++})$$

$$\gamma_{\mathrm{AR}} = \frac{\gamma_0 g \Delta}{16\pi \mathcal{N}} \int d\epsilon f(\epsilon - U^{++}/2) f(-\epsilon - U^{++}/2) \times \left| \sum_{\pm} a(\pm\epsilon + E_C - i\gamma/2) \right|^2, \qquad g \equiv \hbar G/e^2.$$

$$a(\epsilon) = (\epsilon^2 - \Delta^2)^{-1/2} \ln \left[\frac{\Delta - \epsilon + (\epsilon^2 - \Delta^2)^{1/2}}{\Delta - \epsilon - (\epsilon^2 - \Delta^2)^{1/2}} \right]$$

$$\begin{aligned}\mathcal{A} = &\left(\frac{1}{2E_C + 2U^+ - \epsilon_k - \epsilon_l} + \frac{1}{\epsilon_k + \epsilon_l - U^+ - u} \right) \\ &\times [a(\epsilon_k - U^+) + a(\epsilon_l - U^+)] \\ &+ [a(u - \epsilon_k) + a(u - \epsilon_l)] \\ &\times \left(\frac{1}{U^+ + u - \epsilon_k - \epsilon_l} + \frac{1}{2E_C - U^+ - u + \epsilon_k + \epsilon_l} \right)\end{aligned}$$

$$\gamma_{\mathrm{CPE}} = \frac{\gamma_0 g^2 \Delta}{32\pi^2 \mathcal{N}} \int_\Delta^\infty d\Omega \frac{\Omega}{\sqrt{\Omega^2 - \Delta^2}} \int d\epsilon_k \int d\epsilon_l |\mathcal{A}|^2 [1 - f(\epsilon_k)][1 - f(\epsilon_l)] f(\Omega + \epsilon_k + \epsilon_l - U^+ - eV).$$